Supporting Information

***Rec. Nat. Prod*. X:X (202X) XX-XX**

Phytochemical Characterization, Antifungal Activity and Docking Investigation of Isolated Compounds from *Lippia callicarpifolia*

Ana K. Villagómez-Guzmán[1], Ana M. García-Bores[2], Israel Valencia[2], Miriam A. López-Pérez[2], Edgar A. Estrella-Parra [2], José G. Avila-Acevedo[2], Tzasna Hernández-Delgado[1*]

[1]Laboratorio de Bioactividad de Productos Naturales, Unidad de Biotecnología y Prototipos, Facultad de Estudios Superiores Iztacala, Universidad Nacional Autónoma de México, Tlalnepantla, Estado de México 54090, México.

[2]Laboratorio de Fitoquímica, Unidad de Biotecnología y Prototipos, Facultad de Estudios Superiores Iztacala, Universidad Nacional Autónoma de México, Tlalnepantla, Estado de México 54090, México.

Table of Contents **Page**

* Corresponding author: E-Mail: **tzasna@unam.mx**.

Materials and Methods

General Experiment Procedures

The NMR spectra were measured at 300 MHz for ^{1}H and 75.4 MHz for ^{13}C on a Bruker Avance 300 or at 700 MHz for ^{1}H and 175 MHz for ^{13}C on a Bruker Avance III HD 700 MHz spectrometer using chloroform and dimethyl sulfoxide deuterated. HRMS was performed on an Orbitrap Exploris 120 mass spectrometer (Thermo Scientific) by direct infusion. A sample was taken and resuspended in 0.1% formic acid solution in a 1:2 isopropanol: methanol ratio. The acquisition was performed under the following parameters: on Source Type = H-ESI; Spray Voltage: Positive Ion (V) = 3300; Sheath Gas (Arb) = 12; Aux Gas (Arb) = 1; Sweep Gas (Arb) = 0; ion transfer tube temperature (°C) = 320; vaporizer temperature (°C) = 250; Scan Range (*m*/*z*) = 200-1000; FT Resolution = 120000. FTIR spectra were recorded on a Nicolet 6700 FTIR spectrometer. EIMS spectra were recorded at 70 *eV* on a Thermo Scientific GC TRACE 1310 EM ISQLT spectrometer. Column chromatography was performed on silica gel (230-400 mesh). TLC analysis was performed on a precoated gel 60 with fluorescent indicator UV254 (Alugram Xtra Sil), and a sulfuric acid solution (30%) was sprayed with it, followed by heating until colored spots appeared.

Extraction Procedure

The dried and ground leaves/stems of *L. callicarpifolia* (533 g) were extracted by maceration method with 3 L of *n*-hexane, ethyl acetate (EtOAc), and methanol (MeOH), 3 times, in escalating polarity. Following the filtration process, the extracts were concentrated, resulting in the isolation of *n*-hexane (16.1 g), EtOAc (13.3 g), and MeOH (46.2 g) extracts.

The EtOAc extract from the leaves/stems exhibited antifungal activity against *Fusarium sporotrichioides*. The active extract (12.5 g) was chromatographed over silica gel with mixtures of *n*-hexane-EtOAc (1:1) in escalating polarity as eluted to afford 50 fractions. The resulting fractions, which contained a significant yield were evaluated for their antifungal efficacy against *F. sporotrichioides* growth. Fraction 4 (*n*-hexane-EtOAc, 2:3) and fraction 6 (*n*-hexane-EtOAc, 3:7) contained active compounds. Fractions 4 and 5, which exhibited chromatographic similarities (2.3 g), were further fractionated through column chromatography with silica gel and eluted with an *n*-hexane-EtOAc mixture in a 7:3 ratio afforded 15.4 mg of compound **1**. In fraction 6 of the crude extract, a white solid was observed after washing with *n*-hexane-EtOAc (7:3). This procedure afforded 10.6 mg of compound **2**, whereas fraction 39 *n*-hexane-EtOAc (3-4) yielded sugar **3** (8.6 mg).

Ground flowers of *L. callicarpifolia* (241 g) were extracted with 4 L of *n*-hexane, EtOAc, and MeOH, as described above. The resulting extracts were concentrated to yield *n*-hexane (8.6 g), EtOAc (6.9 g), and MeOH (37.4 g) extracts. The EtOAc extract of flowers also exhibited antifungal activity against *F. sporotrichioides*. The extract (6.4 g) was fractionated by column chromatography over silica gel and eluted with an *n-h*exane-EtOAc (7:3) solution with increasing polarity to yield 50 fractions. The fraction 9 (F-9), eluted with *n*-hexane-EtOAc (3:2), and fraction 17 (F-17), eluted with *n*-hexane-EtOAc (1:1), in which the antifungal activity was concentrated, were purified by washing with *n*-hexane-EtOAc (9:1) and CH_2Cl_2, respectively. F-9 yielded 5.1 mg of compound **1**, whereas the F-17 yielded flavone **4** (8.1 mg).

Antifungal Activity

Three yeasts of clinical importance were evaluated: *Candida albicans* 17MR donated by CUSI, FES-Iztacala, UNAM, and *C. glabrata* and *C. tropicalis* were donated by Hospital Angeles Metropolitano, Mexico. *Aspergillus niger*, *Fusarium moniliforme*, *Trichophyton mentagrophytes*, and *Fusarium sporotrichioides* NRLL were donated to the Laboratory of Plant Physiology, UBIPRO, FES-Iztacala. The stock cultures were maintained on potato dextrose agar (PDA, *Bioxon*, Mexico).

The antifungal efficacy of the yeast was assessed using the disk diffusion technique [1]. The inoculum was prepared in sterile Sabouraud Dextrose broth (BD *Bioxon*, Mexico) and incubated

overnight at 37 °C. The inocula (1.5 x 10^8 CFU/mL) were distributed across the surface of the PDA agar. Subsequently, paper disks saturated with 2 mg/disk of each extract were placed and incubated at 37 °C for 24 h. Nystatin (20.6 μg/disk, *Bio-Rad*, France) as the positive control.

The antifungal activity of the extracts, fractions, and isolated compounds against molds was evaluated according to the radial growth inhibition method described by Serrano et al. [2], with some modifications. The Petri dishes were filled with 25 mL of PDA. A fungal disc (5 mm diameter) containing conidia from each examined strain was placed at the center of each dish. Paper disks containing 2 mg/disk of each extract. The Petri dishes were incubated for 14 days until mycelial growth developed at room temperature. Ketoconazole (60 μg/mL) was used as a positive control, and solvent-negative controls were also used.

For the determination of quantitative concentration, six varying concentrations of extracts (4, 2, 1, 0.5, 0.250, and 0.125 mg/mL), fractions (4, 2, 1, mg/mL), and compounds **1** and **4** (1, 0.5 and 0.25 mg/mL) were subjected to assays [2].

In the quantitative assays of the extracts, fractions, or pure compounds, the specified doses were dissolved in dimethyl sulfoxide (0.5%) and acetone (1%) and rapidly mixed with PDA agar (3 mL), and poured into a 24-well (1 mL) in triplicate. Once the agar had cooled, the conidia were inoculated at 1x10^4 conidia/5 μL. The Petri dishes were maintained at room temperature for an extended time of 72 hours to facilitate mycelium development. The positive control for the experiment was ketoconazole at of 60 μg/mL, with the solvent for extract dilutions functioning as the negative control. Once the incubation period was completed, measurement of fungal growth inhibition was measured using the following formula:

$$I\ (\%) = (dc - dt) / dc \times 100$$

Here, I (%) stands for the percentage of inhibition, with dc representing the diameter of the control culture colony and dt denoting the diameter of the treated culture colony.

Statistical Analysis

All analyses were performed in triplicate, and the assay results are reported as mean ± standard deviation using the Microsoft Excel program.

Docking Analysis

The ligand was initially optimized using Gaussian16 software [3] and the Density Functional Theory (DFT) with the B3LYP method [4]. Subsequently, the three-dimensional structure of the 1JFA protein, trichodiene synthase from *F. sporotrichioides*, was obtained from the Protein Data Bank (PDB), [5]. This enzyme catalyzes the cyclization of farnesyl diphosphate to produce trichodiene, a key intermediate in the biosynthesis of trichothecene mycotoxins. Homology was performed using the YASARA software [6].

The CavityPlus [7-8] software, which is tailored for robust protein cavity detection and functional analysis, was subsequently used. This tool detects potential binding sites on the protein surface and ranks them according to druggability score. Residues from the binding site labeled with a "strong" druggability description were then isolated, and the box was defined in the Vina program [9-10] to adjust both the ligand center and box size. Virtual screening was then performed using Vina exclusively for ligands with negative binding affinity [11-12]. The figures were generated using the PyMOL Molecular Graphics System version 2.0. Schrödinger.

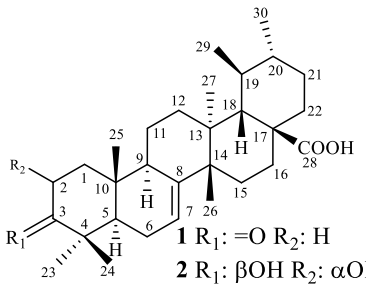

1 R_1: =O R_2: H

2 R_1: βOH R_2: αOH

Table S1 : NMR data for *D:C*-friedours-7-en-28-oic-acid compounds **1** in $CDCl_3$ and **2** in DMSO-d_6 compared with the analogous structure.

No	**1**			***D:C*-3-oxo-friedours-7-en-28-oic acid** [11]	***D:C*-friedours-7-en-3-one** [13]		**2**		
	δ_H, mult, *J* in Hz	δ_C	HMBC	δ_H, mult, *J* in Hz	δ_C	δ_H, mult, *J* in Hz	δ_H, mult, *J* in Hz	δ_C	HMBC[a]
1	1.98, m; 1.46, m	38.2	25	-	38.31	1.98; 1.43	1.84, dd, 10.4, 2.3; 1.19, m	42.5	25
2	2.76, ddd, 14.6, 14.6, 5.7; 2.26, m	34.9	-	2.761, ddd, *J*= 14.8, 14.8, 5.4	34.89	2.75; 2.25	3.87, m	70.1	1
3	-	216.9	23, 24	-	216.64	-	2.99, d, 2.1	77.3	1, 23, 24
4	-	47.8	5, 23, 24	-	47.77	-	-	37.8	5, 23, 24,
5	1.72, t, 8.9	52.1	23, 24, 25	-	52.17	1.72	1.32, m	50.0	23, 24, 25
6	2.33, m; 2.12, m	24.5	5	-	24.57	2.13; 2.10	2.08, m; 1.98, m	23.8	5
7	5.47, m	116.9	-	5.463, m	116.43	5.51	5.41, m	116.8	6
8	-	144.7	26	-	145.46	-	-	144.0	6, 11, 26
9	2.33, m	47.9	25	-	47.86	2.30	2.17, m	48.2	5, 25
10	-	35.3	25	-	35.28	-	-	34.2	1, 5, 25
11	1.64, m	16.5	-	-	17.00	1.55	1.53, m	15.9	12
12	1.64, m	32.5	27	-	32.40	1.52	1.55, m; 1.26, m	32.0	27
13	-	37.1	18, 26, 27	-	37.77	-	-	36.6	18, 26, 27
14	-	41.1	26, 27	-	41.40	-	-	40.6	16, 26, 27
15	1.58, m	28.3	26	-	28.96	1.55; 1.46	1.28, m	28.9	16, 26
16	1.93, m; 1.48, m	32.5	-	-	37.68	1.51; 1.19	1.74, td, 9.8, 4.0; 1.51, m	32.2	18
17	-	44.7	18, 27	-	32.03	-	-	43.8	16, 18
18	2.37, brs	47.5	27	-	54.99	1.30	2.31, brs	47.6	27, 29
19	1.15, m	36.7	29, 30	-	35.39	1.16	1.07, m	36.2	18, 29, 30
20	1.12, m	32.3	30	-	32.03	1.56	1.07, m	31.6	29, 30
21	1.13, m	28.9	30	-	29.22	1.29	1.52, m; 1.46, m	27.8	30
22	2.27, m; 1.68, m	26.0	-	-	31.56	1.57; 1.18	2.19, m; 1.60, m	25.6	16
23	1.05, s	24.4	24	1.064	24.50	1.04	0.86, s	29.2	5, 24
24	1.11, s	21.5	23	1.110	21.45	1.11	0.98, s	16.7	5, 23
25	1.01, s	12.6	-	1.030	12.66	1.01	0.92, s	14.1	1, 5
26	1.11, s	23.6	-	1.102	23.79	1.03	1.01, s	23.3	18
27	1.04, s	21.9	-	1.040	22.72	0.95	0.98, s	21.4	18
28	-	186.3	-	-	37.99	1.04	-	181.6	16, 18, 22
29	1.06, d, 6.9	23.4	-	1.007, brs	25.65	1.05	1.00, d, 6.0	23.2	18
30	0.87, d, 3.6	21.3	-	0.86, d, *J*= 4.9	22.52	0.90	0.82, d, 2.7	21.2	21

Measured at 300 MHz for ^1H and 75.4 MHz for ^{13}C. [a]HMBC correlations of compound 2 were observed at 300 and 700 MHz.

Table S2: Bonding interactions of genkwanin with IJFA protein trichodiene synthase residues.

Hydrogen bond	Hydrophobic interactions
LYS-198	PHE-142
PHE-114	PRO-144
	MET-110
	LEU-148
	VAL-111
	ARG-140
	ASN-112
	TYR-113
	ILE-151
	PRO-136
	PHE-114
	ASP-115

References

[1] CLSI (2018). Performance standards for antimicrobial disk susceptibility test: Approved standard, Clinical and Laboratory Standard Institute, National Committee for Clinical and Laboratory Standards **38**, 1-72.

[2] R. Serrano, T. Hernández, M. Canales, A. M. García-Bores, A. R. De Vivar, C. L. Cespedes and J. G. Avila (2009). Ent-labdane type diterpene with antifungal activity from *Gymnosperma glutinosum* (Spreng.) Less. (Asteraceae), *Bol. Latinoam. Caribe Plantas Med. Aromat*. **8**, 412-418.

[3] M. J. Frisch, G. W. Trucks, H. B. Schlegel, et al. (2016). Gaussian 16, Revision A.03, Gaussian, Inc., Wallingford CT.

[4] A. D. Becke (1993). Density-functional thermochemistry. III. The role of exact exchange, *J. Chem. Phys.* **98**, 5648-5652.

[5] H. M. Berman, J. Westbrook, Z. Feng, G. Gilliland, T. N. Bhat, H. Weissig, I. N. Shindyalov and P. E. Bourne. The Protein Data Bank, *Nucleic Acids Res*. **28**, 235-242.

[6] E. Krieger, G. Koraimann and G. Vriend (2002). Increasing the precision of comparative models with YASARA NOVA—a self-parameterizing force field, Proteins, *Struct. Funct. Bioinf.* **47**, 393-402.

[7] S. Wang, J. Xie, J. Pei and L. Lai (2023). CavityPlus 2022 update: an integrated platform for comprehensive protein cavity detection and property analyses with user-friendly tools and cavity databases, *J. Mol. Biol.* **435,** 168141.

[8] Y. Xu, S. Wang, Q. Hu, S. Gao, X. Ma, W. Zhang and J. Pei (2018). CavityPlus: a web server for protein cavity detection with pharmacophore modelling, allosteric site identification and covalent ligand binding ability prediction, *Nucleic Acids Res*. **46**, W374-W379.

[9] J. Ding, S. Tang, Z. Mei, L. Wang, Q. Huang, H. Hu and J. Wu (2023). Vina-GPU 2.0: further accelerating AutoDock Vina and its derivatives with graphics processing units, *J. Chem. Inf. Model*. **63**, 1982-1998.

[10] S. Tang, R. Chen, M. Lin, Q. Lin, Y. Zhu, J. Ding, H. Hu, M. Ling and J. Wu (2022). Accelerating AutoDock Vina with GPUs, *Molecules*, **27**, 3041.

[11] J. Eberhardt, D. Santos-Martins, A. F. Tillack and S. Forli (2021). AutoDock Vina 1.2.0: New docking methods, expanded force field, and Python bindings, *J. Chem. Inf. Model*. **61**, 3891-3898.

[12] O. Trott and A. J. Olson (2010). AutoDock Vina: improving the speed and accuracy of docking with a new scoring function, efficient optimization, and multithreading, *J. Comput. Chem*. **31**, 455-461.

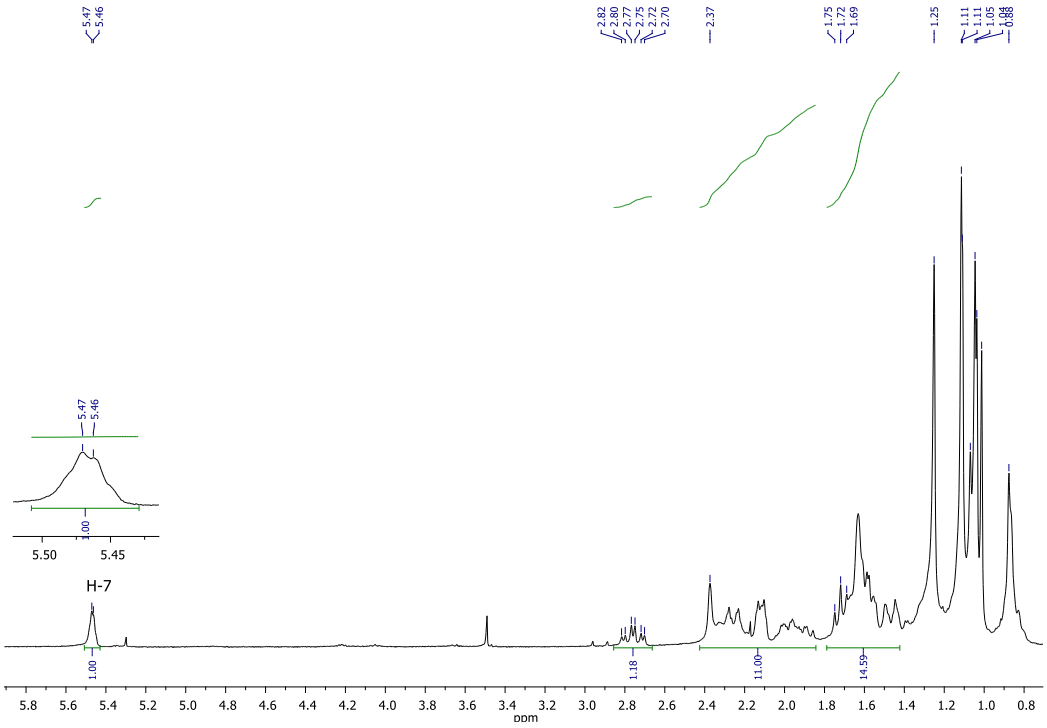

Figure S1: [1]H NMR spectrum of *D:C*-3-oxo-friedours-7-en-28-oic acid (**1**) in $CDCl_3$ (300 MHz).

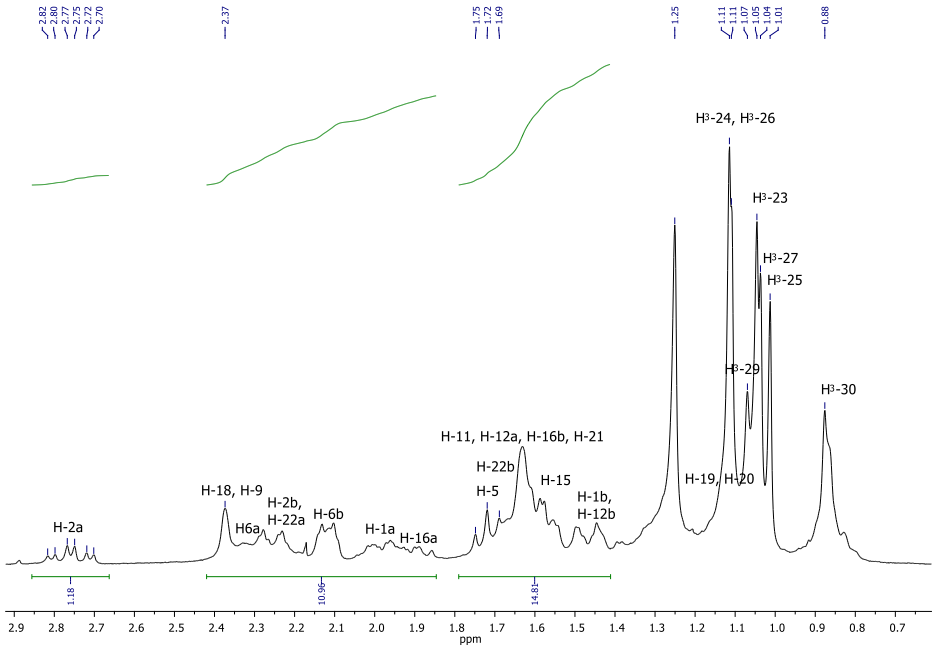

Figure S1a: Extended [1]H NMR spectrum of *D:C*-3-oxo-friedours-7-en-28-oic acid (**1**) in $CDCl_3$ (300 MHz).

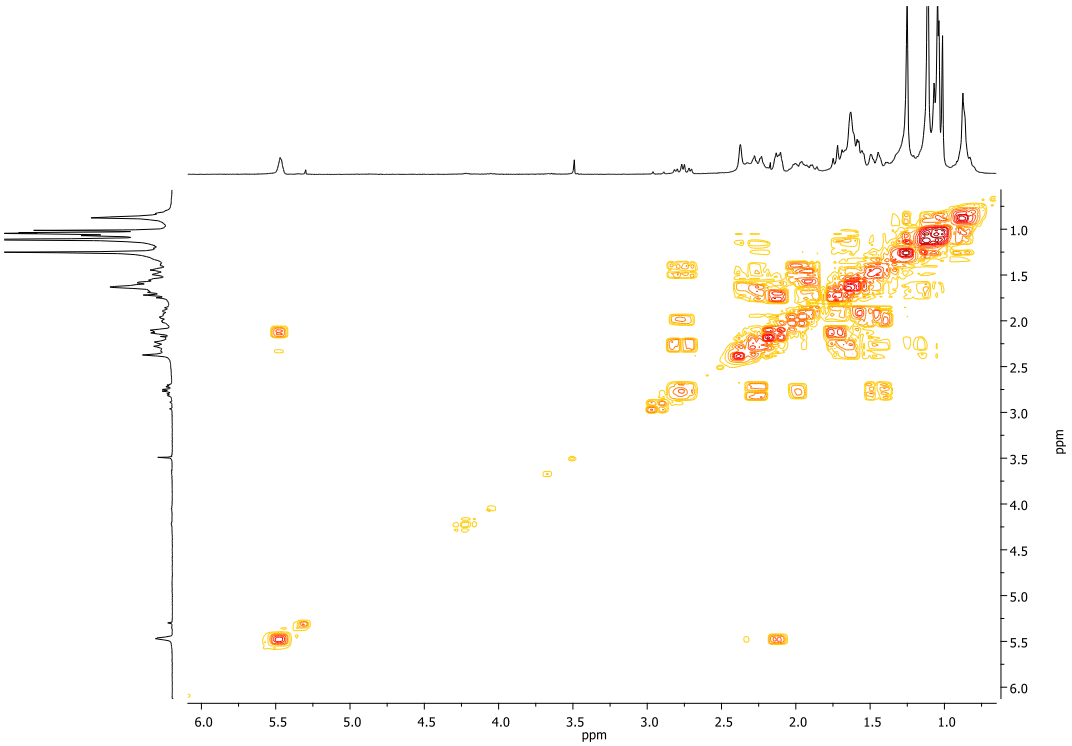

Figure S2: COSY spectrum of *D:C*-3-oxo-friedours-7-en-28-oic acid (**1**) in $CDCl_3$.

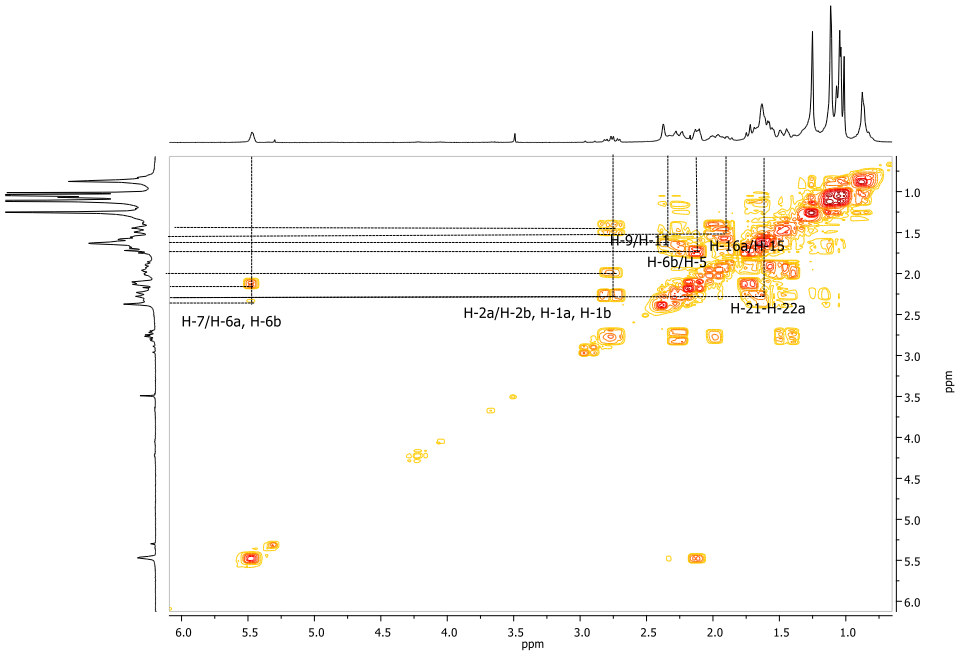

Figure S2a: Extended COSY spectrum of *D:C*-3-oxo-friedours-7-en-28-oic acid (**1**) in $CDCl_3$.

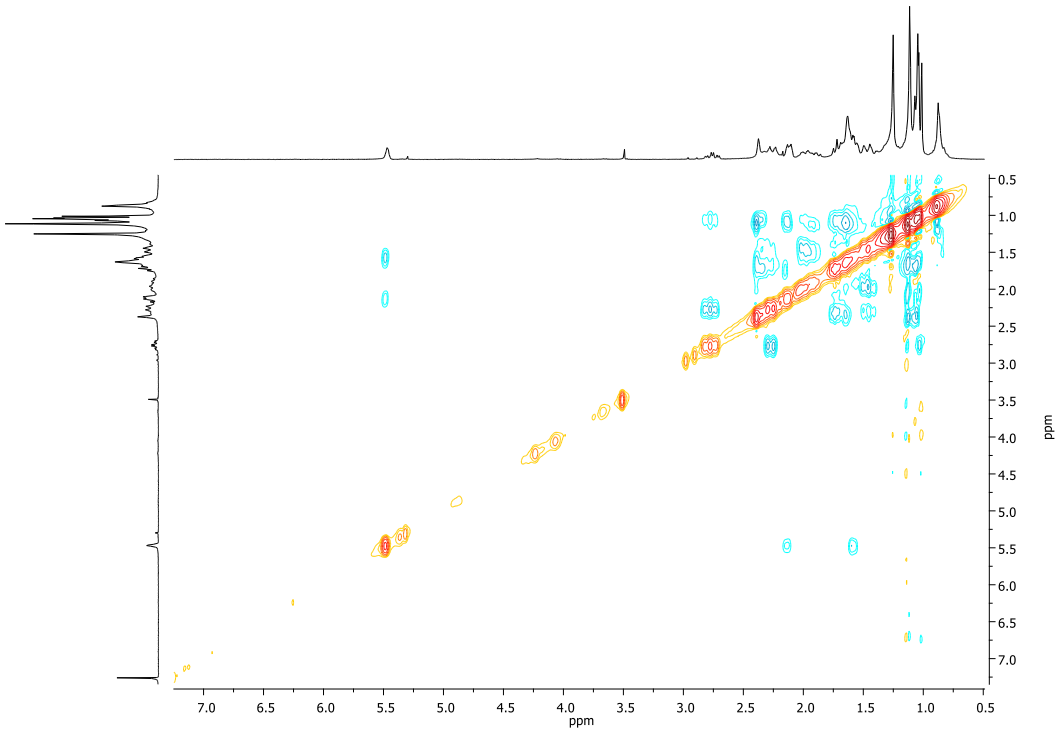

Figure S3: NOESY spectrum of *D:C*-3-oxo-friedours-7-en-28-oic acid (**1**) in $CDCl_3$.

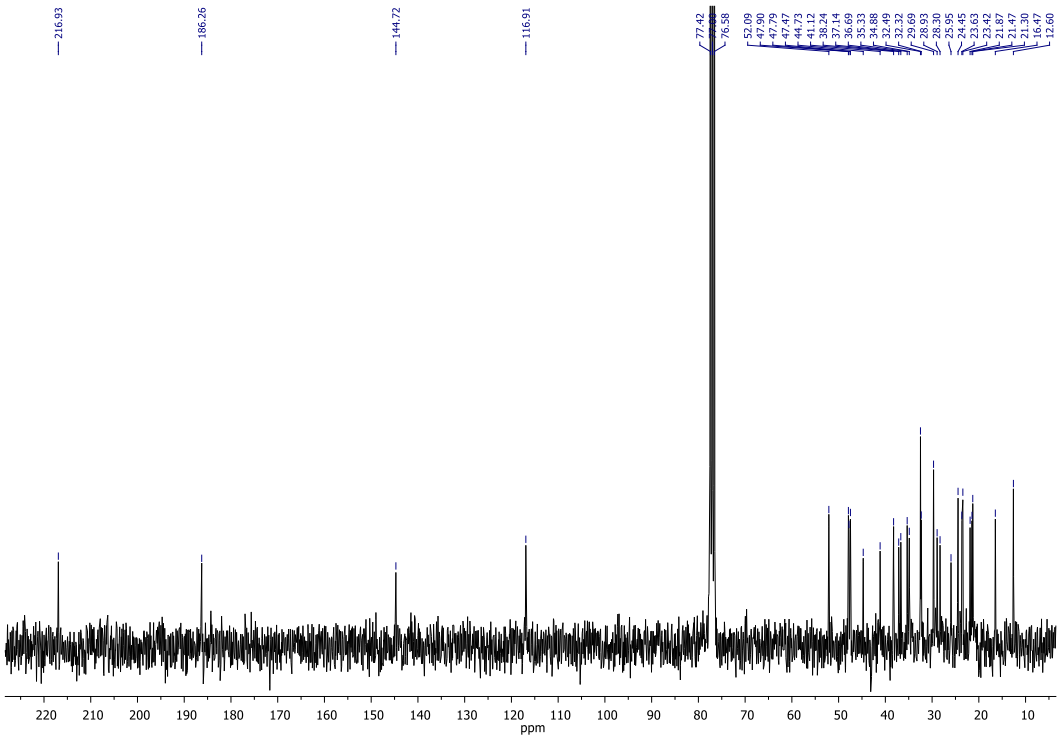

Figure S4: ^{13}C NMR spectrum of *D:C*-3-oxo-friedours-7-en-28-oic acid (**1**) in $CDCl_3$ (75 MHz).

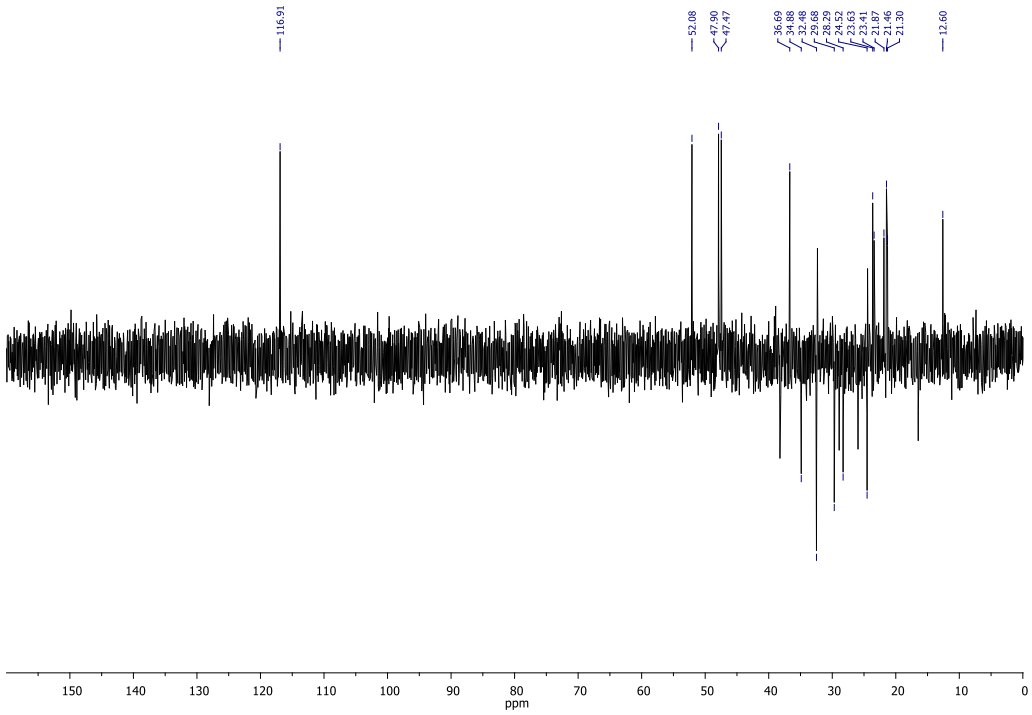

Figure S5: DEPT spectrum of *D:C*-3-oxo-friedours-7-en-28-oic acid (**1**) in $CDCl_3$.

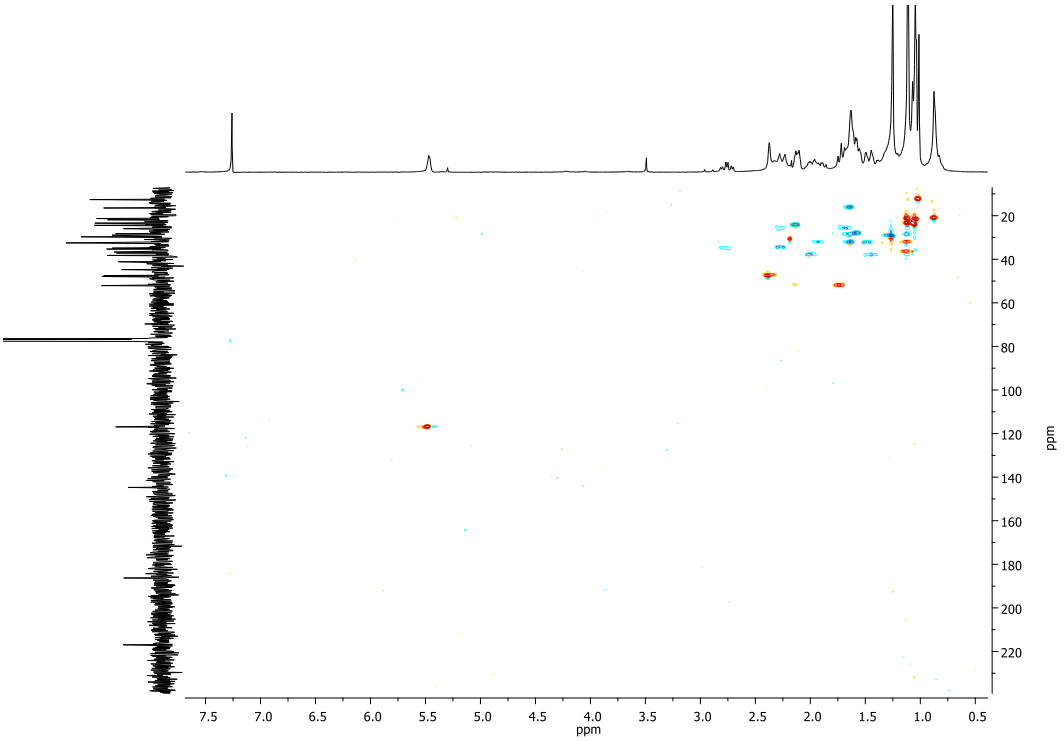

Figure S6: HSQC spectrum of *D:C*-3-oxo-friedours-7-en-28-oic acid (**1**) in $CDCl_3$.

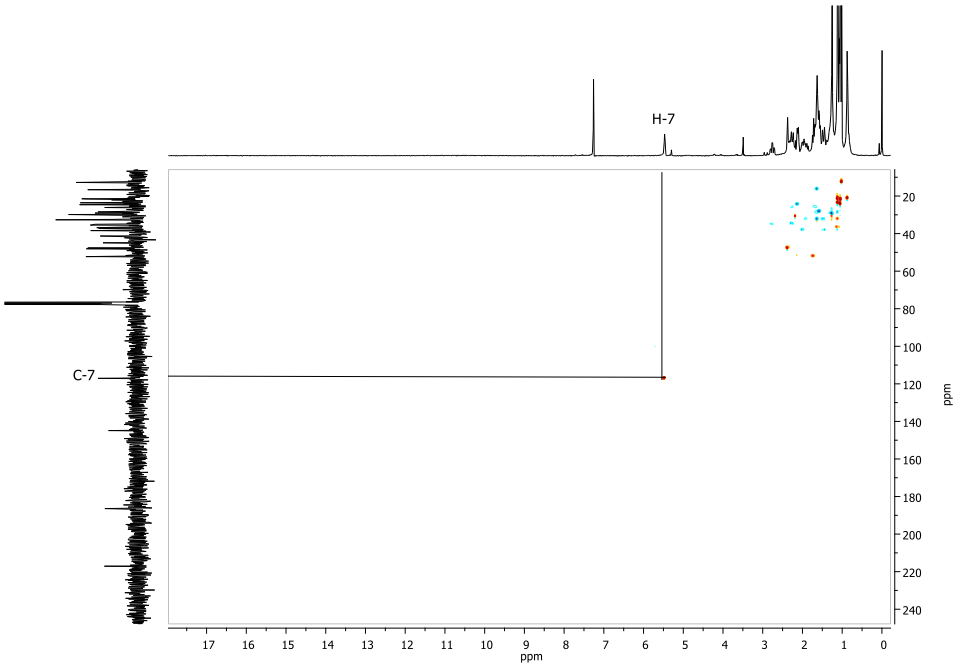

Figure S6a: Extended HSQC spectrum of *D:C*-3-oxo-friedours-7-en-28-oic acid (**1**) in $CDCl_3$.

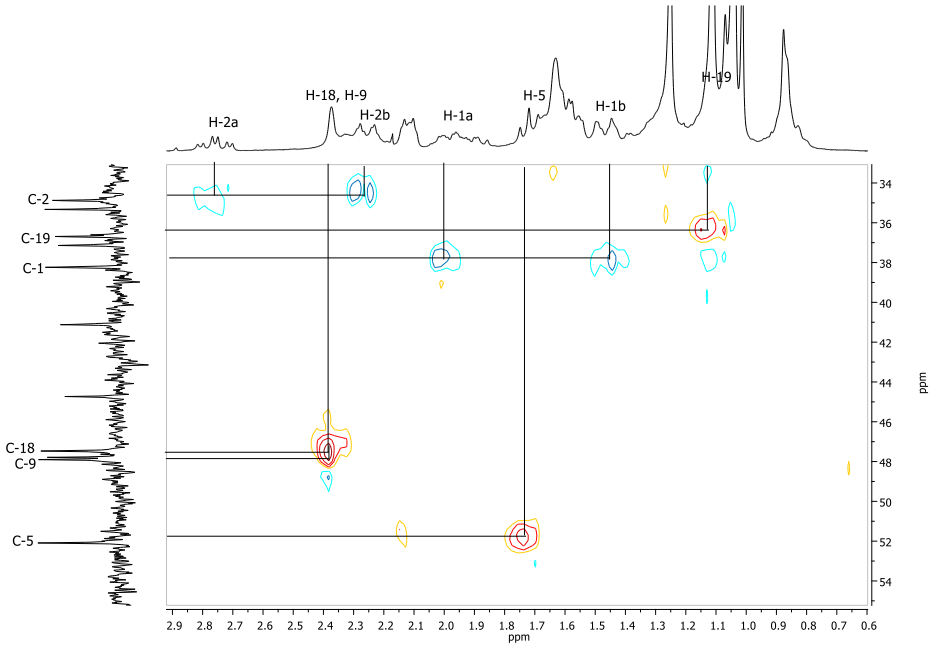

Figure S6b: Extended HSQC spectrum of *D:C*-3-oxo-friedours-7-en-28-oic acid (**1**) in $CDCl_3$.

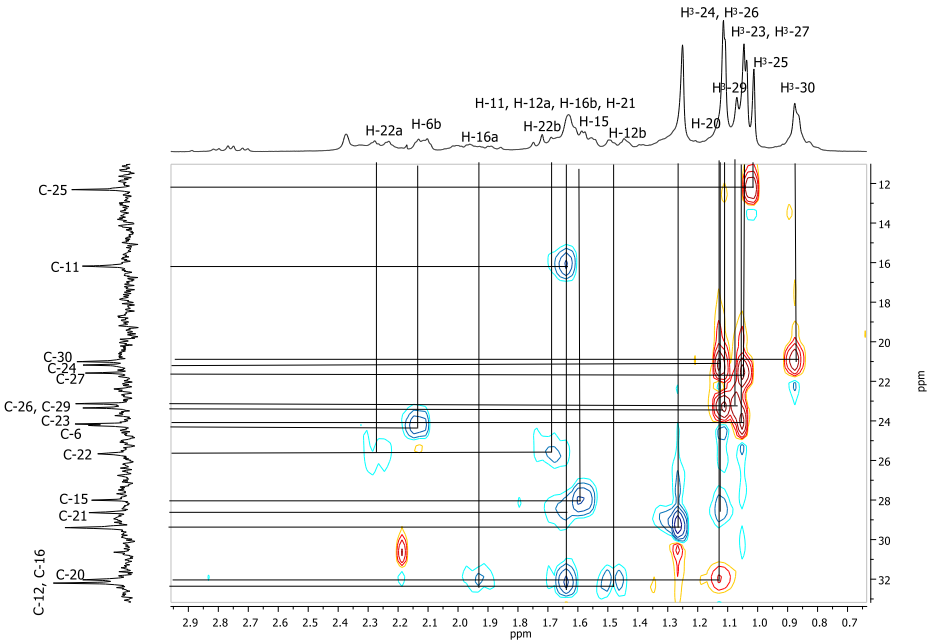

Figure S6c: Extended HSQC spectrum of *D:C*-3-oxo-friedours-7-en-28-oic acid (**1**) in $CDCl_3$.

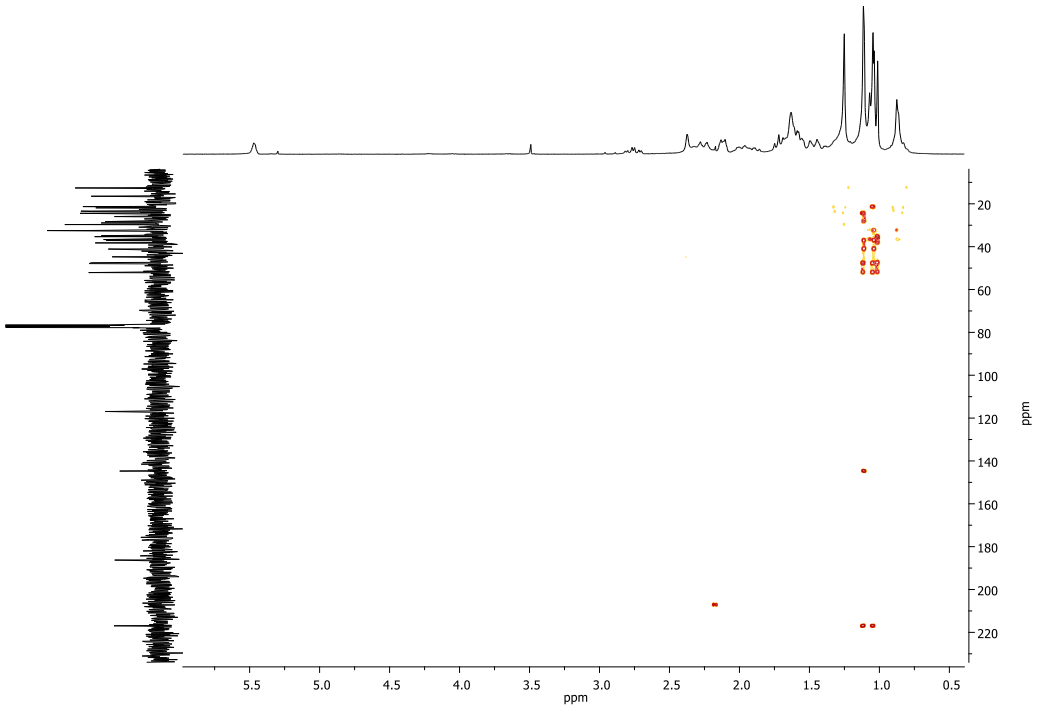

Figure S7: HMBC spectrum of *D:C*-3-oxo-friedours-7-en-28-oic acid (**1**) in $CDCl_3$.

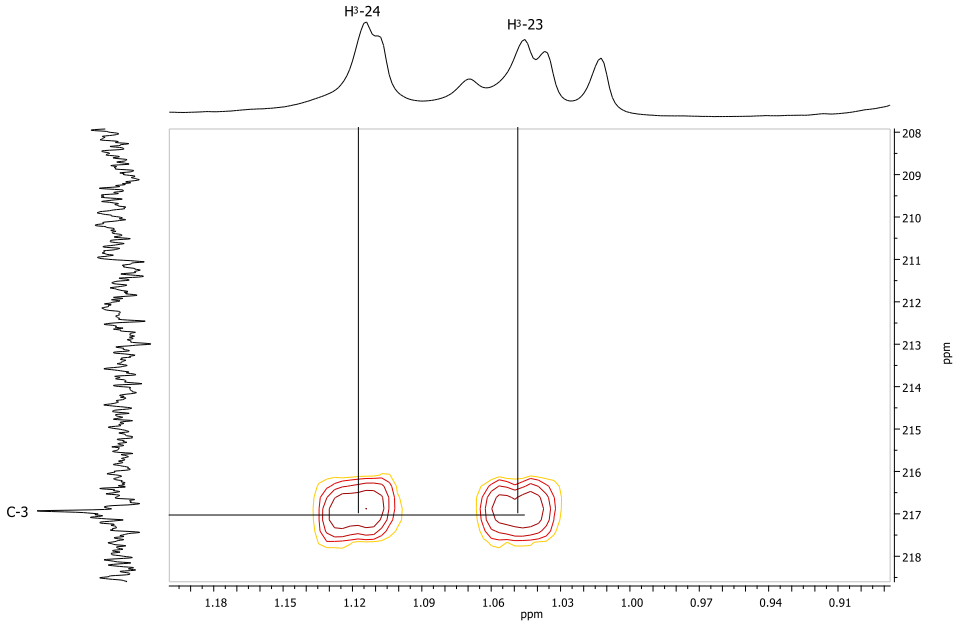

Figure S7a: Extended HMBC spectrum of *D:C*-3-oxo-friedours-7-en-28-oic acid (**1**) in $CDCl_3$.

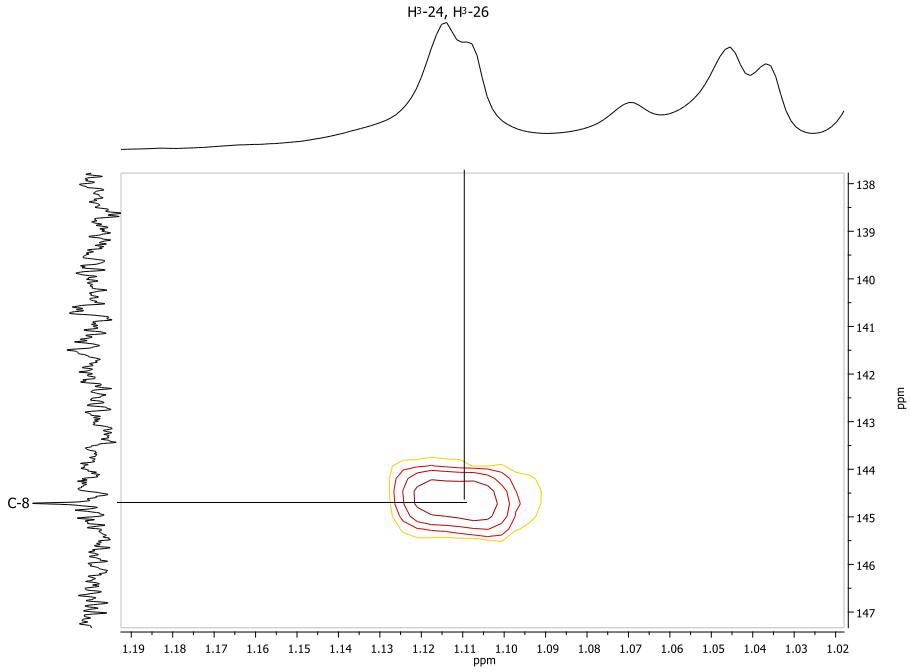

Figure S7b: Extended HMBC spectrum of *D:C*-3-oxo-friedours-7-en-28-oic acid (**1**) in $CDCl_3$.

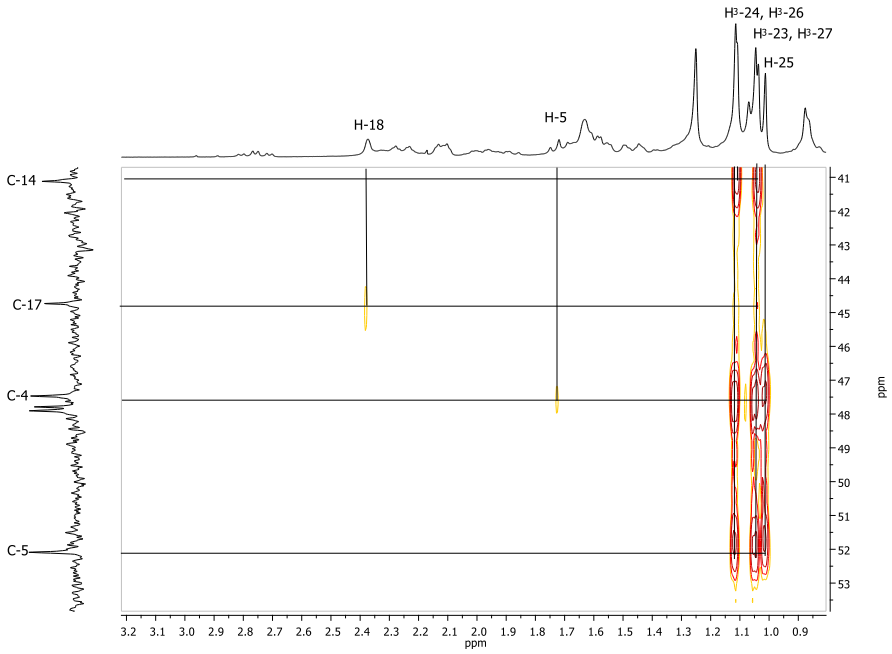

Figure S7c: Extended HMBC spectrum of *D:C*-3-oxo-friedours-7-en-28-oic acid (**1**) in $CDCl_3$.

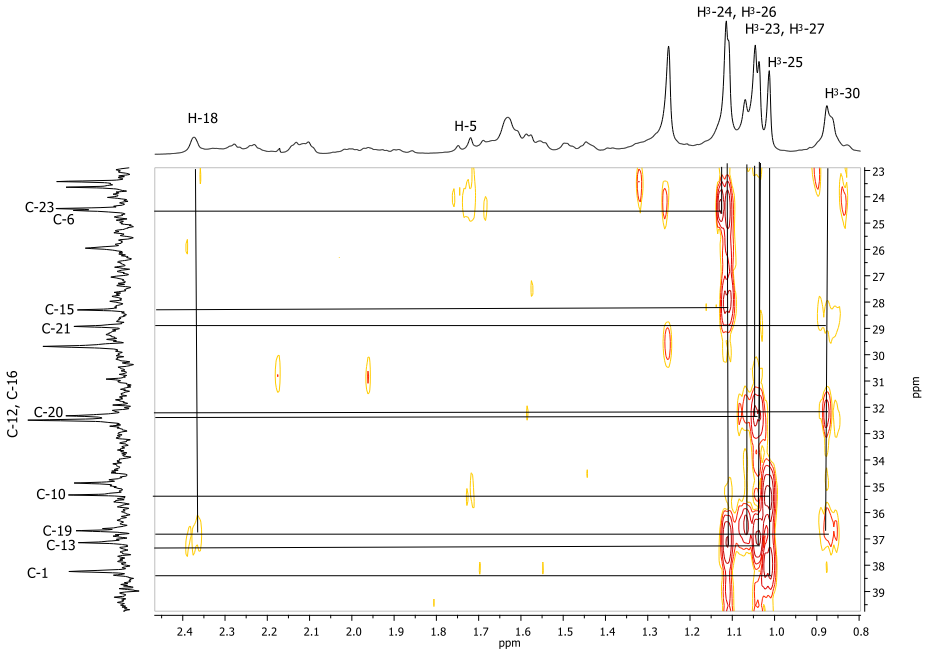

Figure S7d: Extended HMBC spectrum of *D:C*-3-oxo-friedours-7-en-28-oic acid (**1**) in $CDCl_3$.

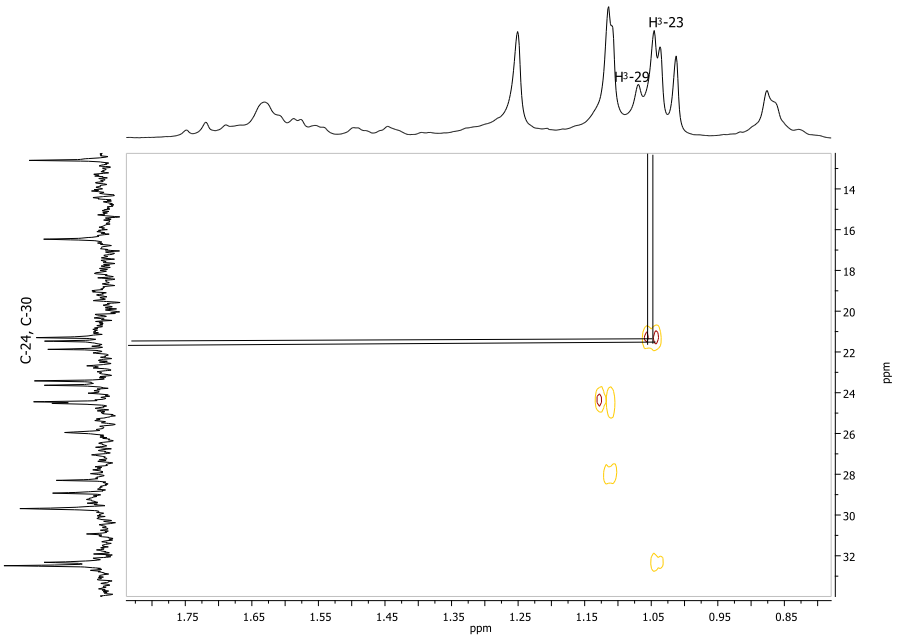

Figure S7e: Extended HMBC spectrum of *D:C*-3-oxo-friedours-7-en-28-oic acid (**1**) in $CDCl_3$.

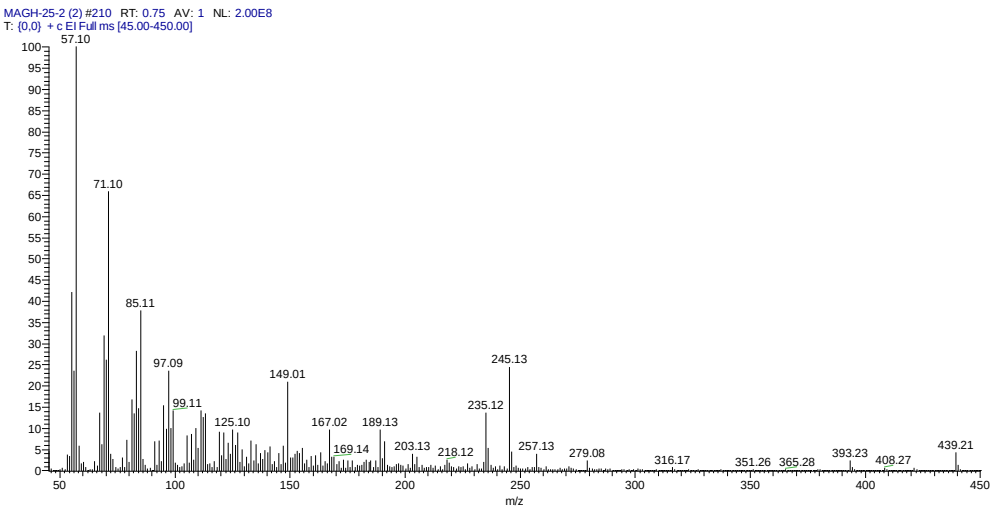

Figure S8: EIMS spectrum of *D:C*-3-oxo-friedours-7-en-28-oic acid (**1**) at 70 *eV*.

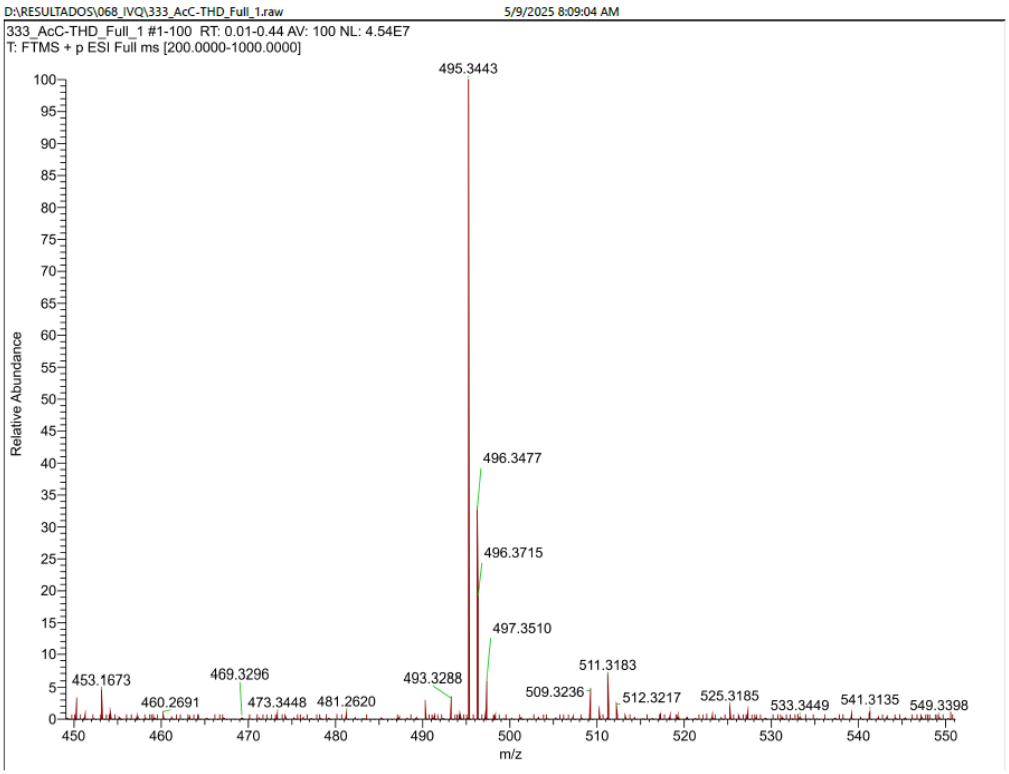

Figure S9: Extended HRMS spectrum of callicarpifolic acid (**2**) from 450-550 *m/z*.

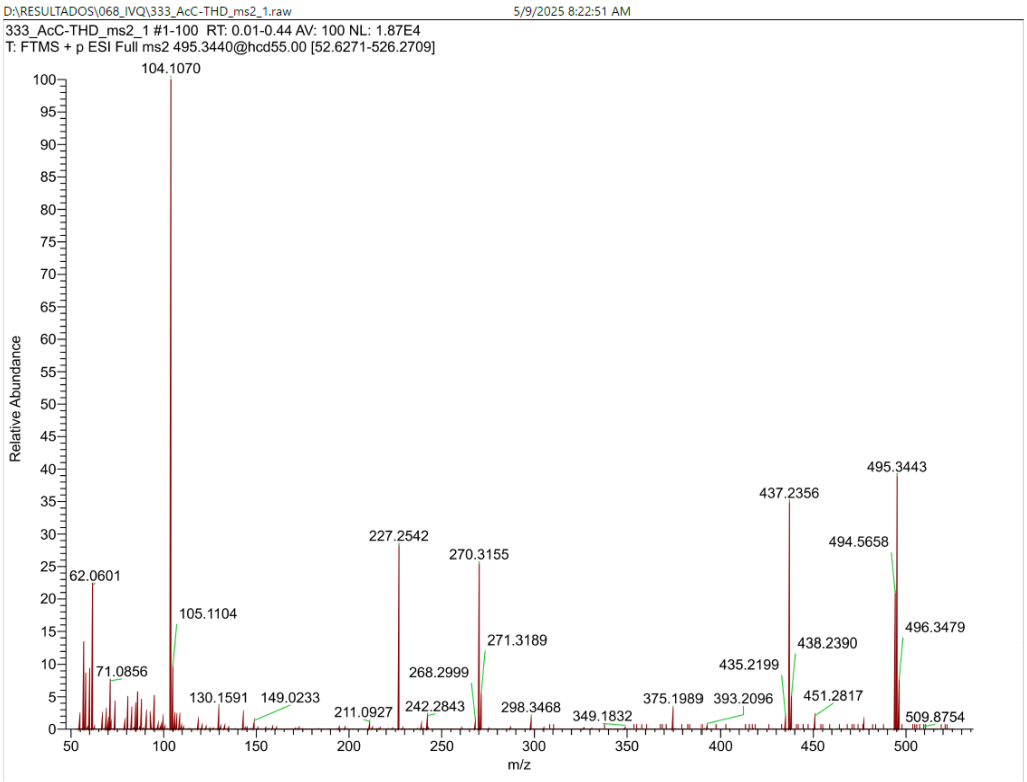

Figure S10: Fragmentation spectrum of the callicarpifolic acid (**2**) ion observed in the full scan.

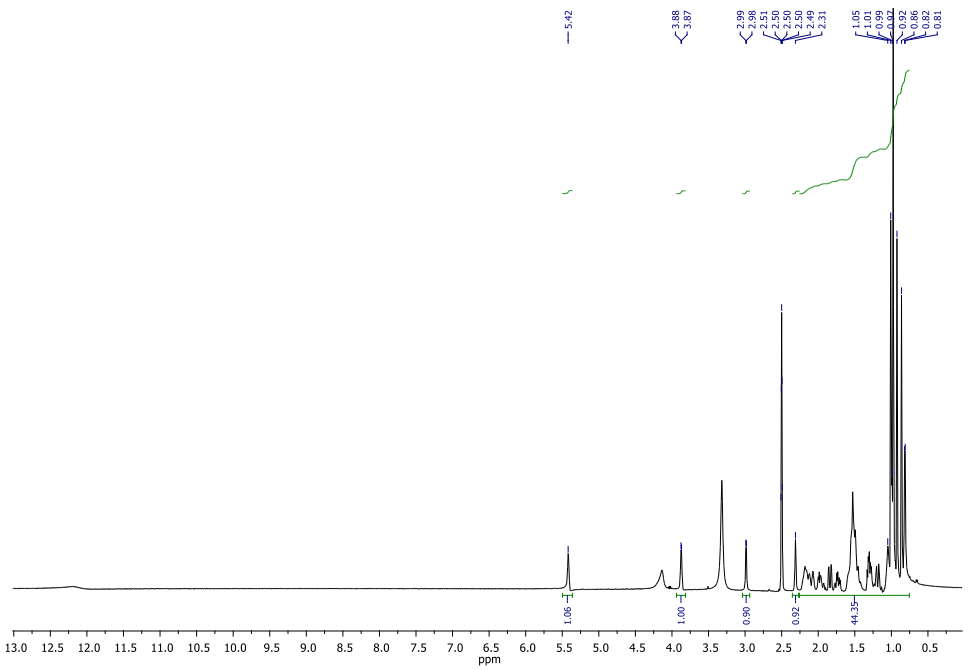

Figure S11: [1]H NMR spectrum of callicarpifolic acid (**2**) in DMSO-d_6 (300 MHz).

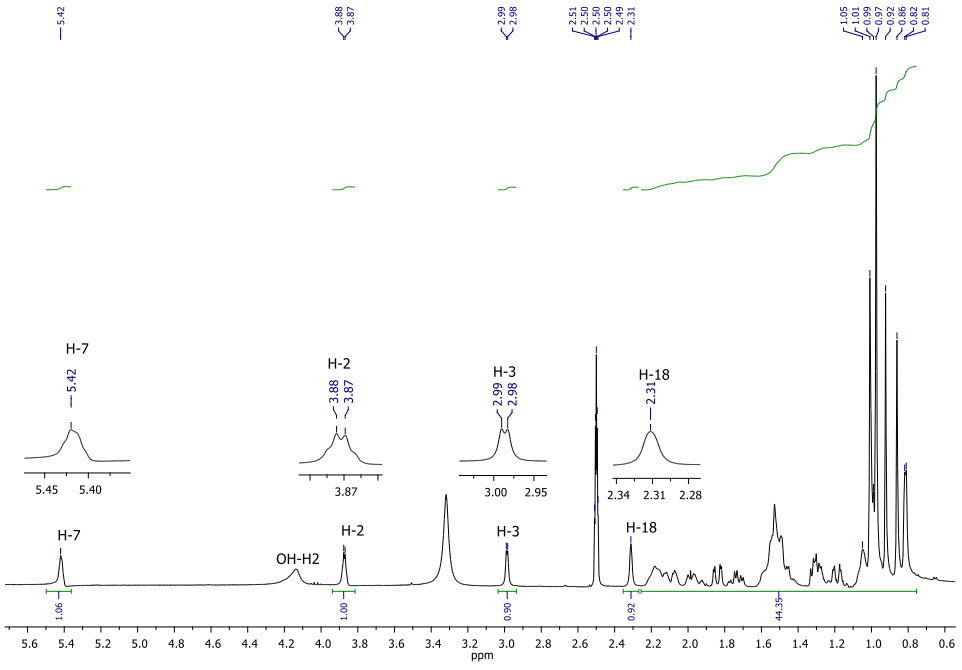

Figure S11a: Extended [1]H NMR spectrum of callicarpifolic acid (**2**) in DMSO-d_6 (300 MHz).

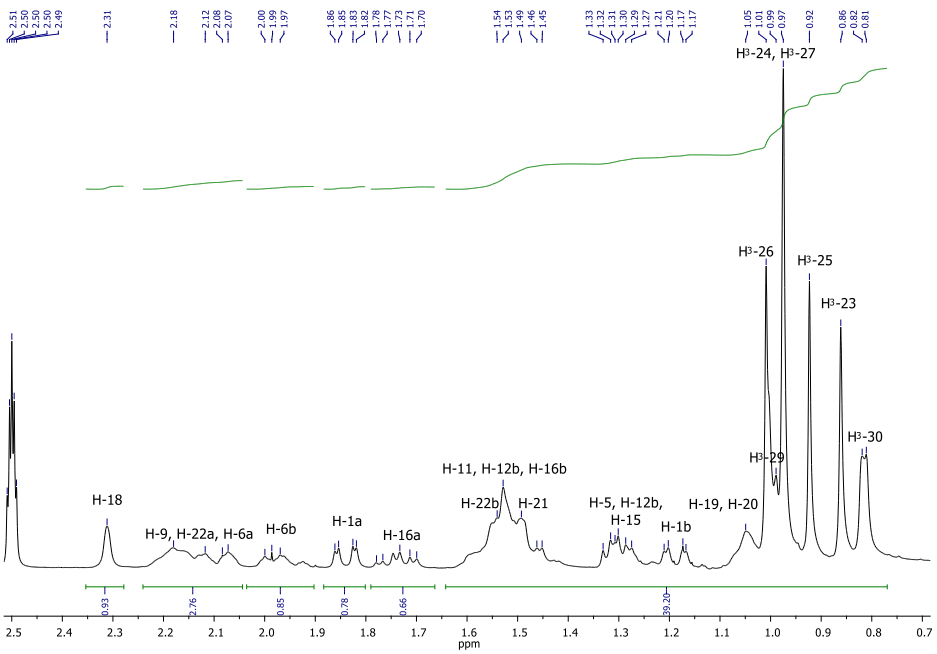

Figure S11b: Extended [1]H NMR spectrum of callicarpifolic acid (**2**) in DMSO-d_6 (300 MHz).

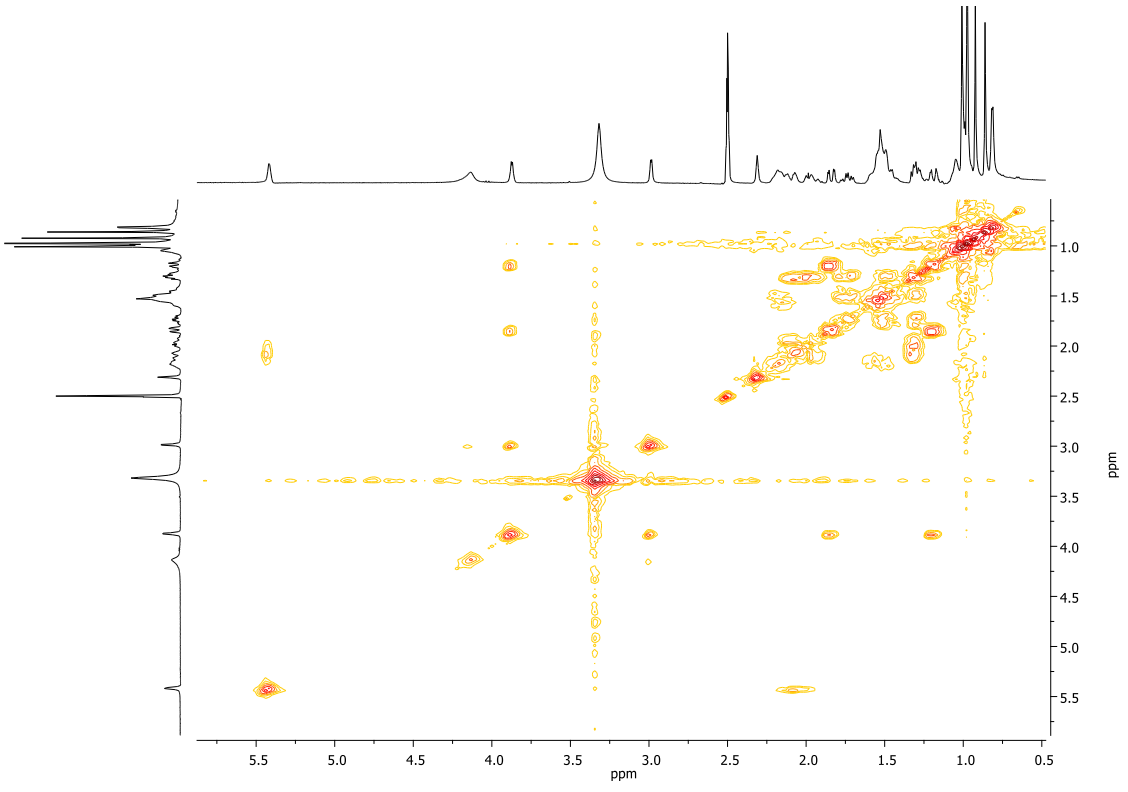

Figure S12: COSY spectrum of callicarpifolic acid (**2**) in DMSO-d_6.

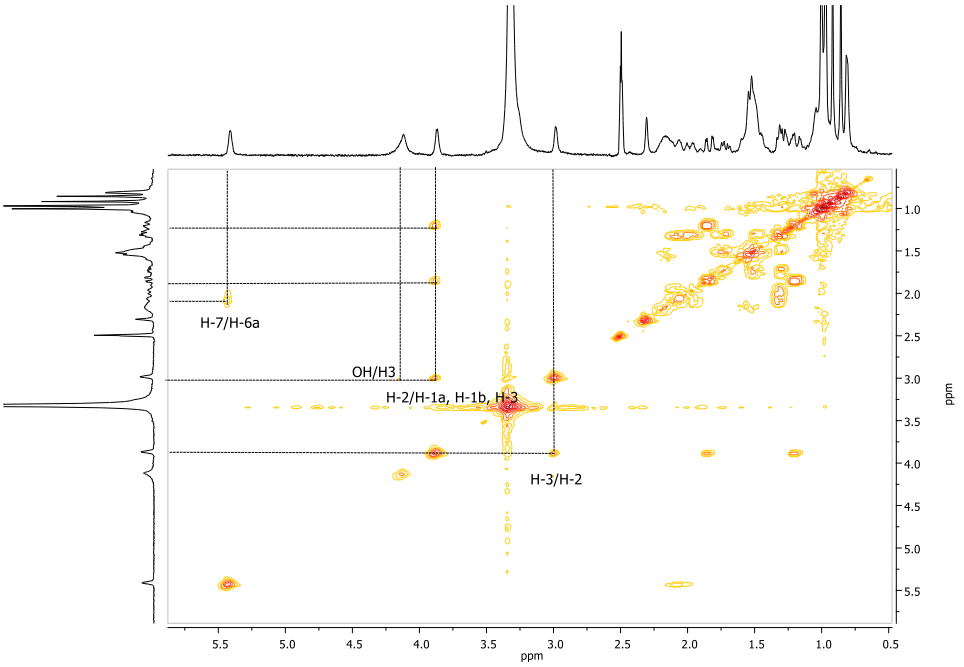

Figure S12a: Extended COSY spectrum of callicarpifolic acid (**2**) in DMSO-d_6.

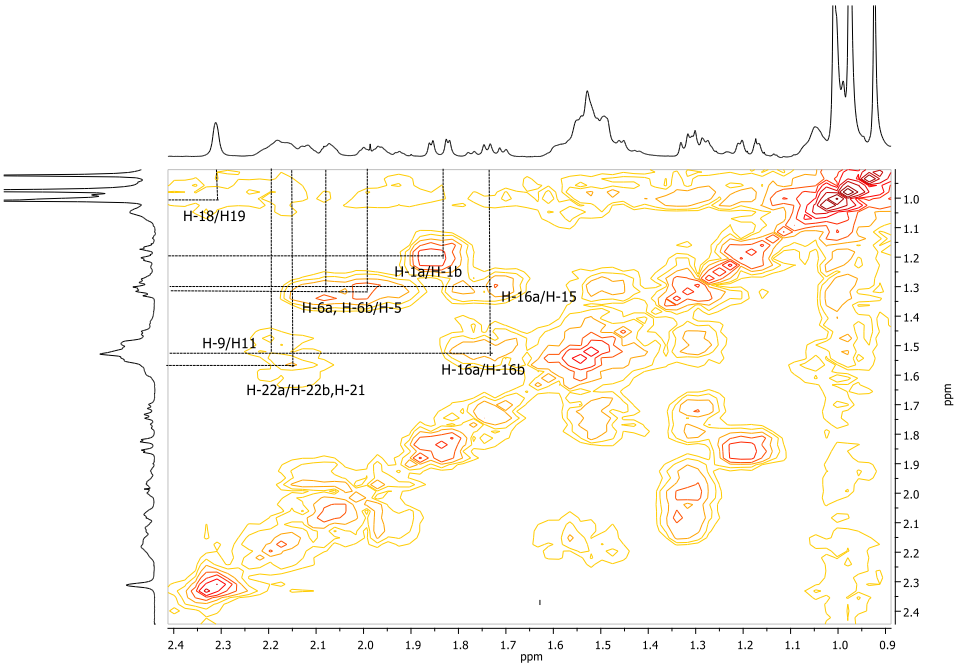

Figure S12b: Extended COSY spectrum of callicarpifolic acid (**2**) in DMSO-d_6.

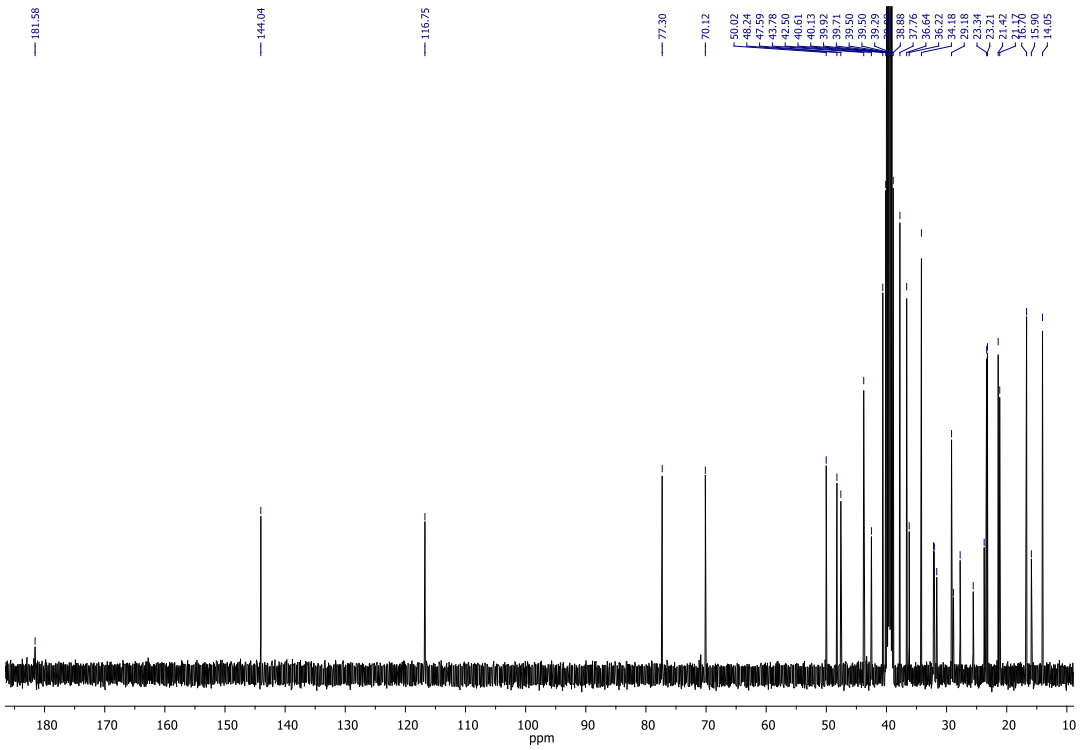

Figure S13: ^{13}C NMR spectrum of callicarpifolic acid (**2**) in DMSO-d_6 (75.4 MHz).

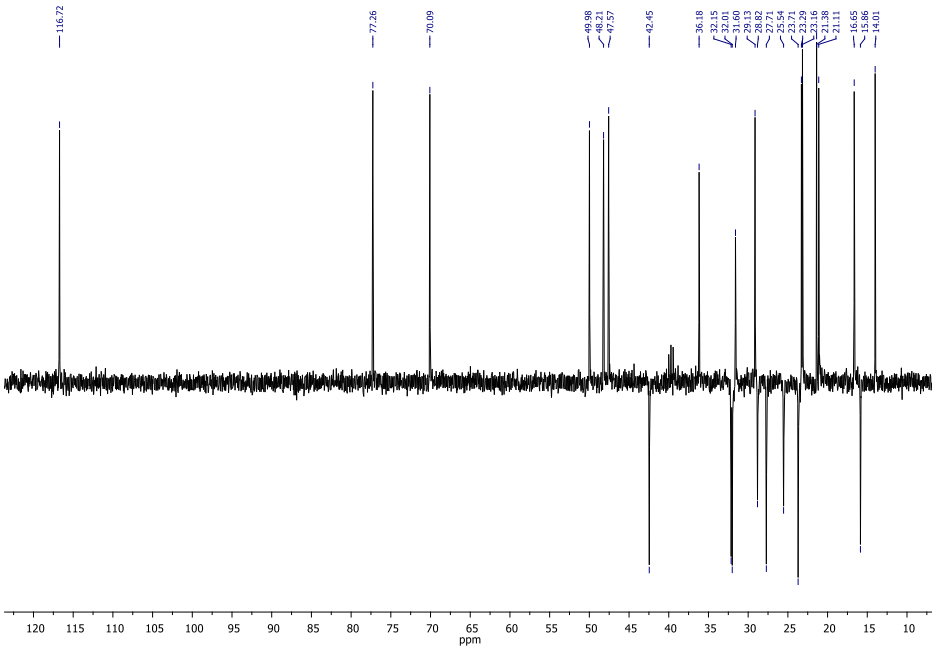

Figure S14: DEPT spectrum of callicarpifolic acid (**2**) in DMSO-d_6.

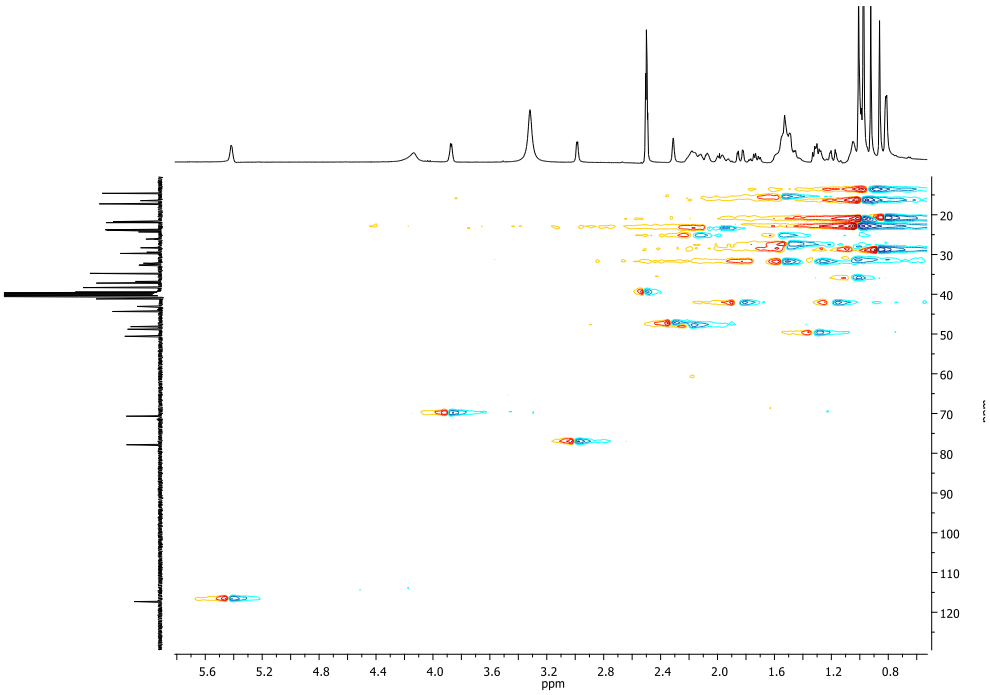

Figure S15: HSQC spectrum of callicarpifolic acid (**2**) in DMSO-d_6.

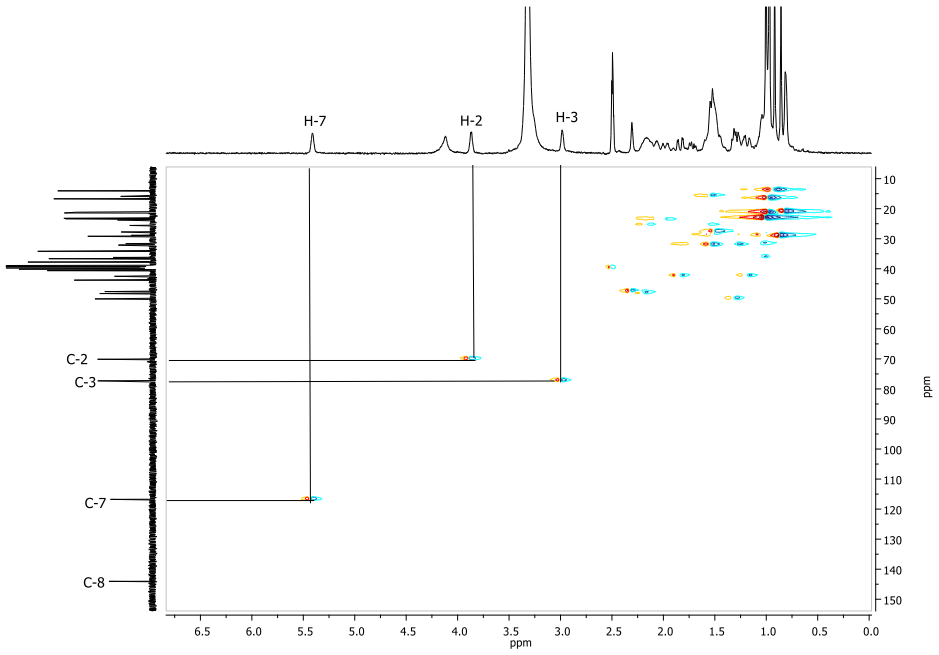

Figure S15a: Extended HSQC spectrum of callicarpifolic acid (**2**) in DMSO-d_6.

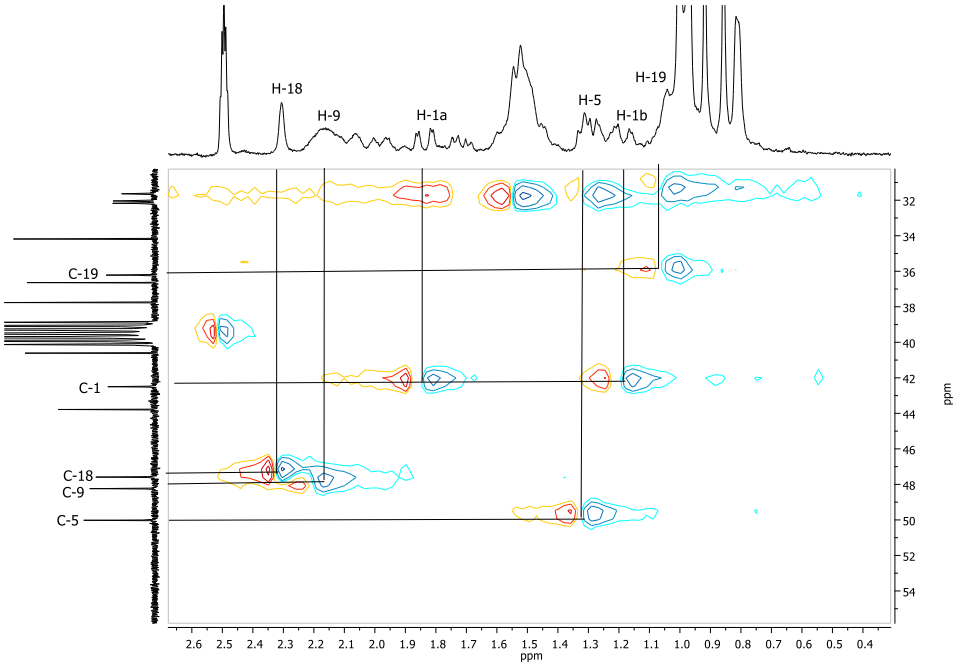

Figure S15b: Extended HSQC spectrum of callicarpifolic acid (**2**) in DMSO-d_6.

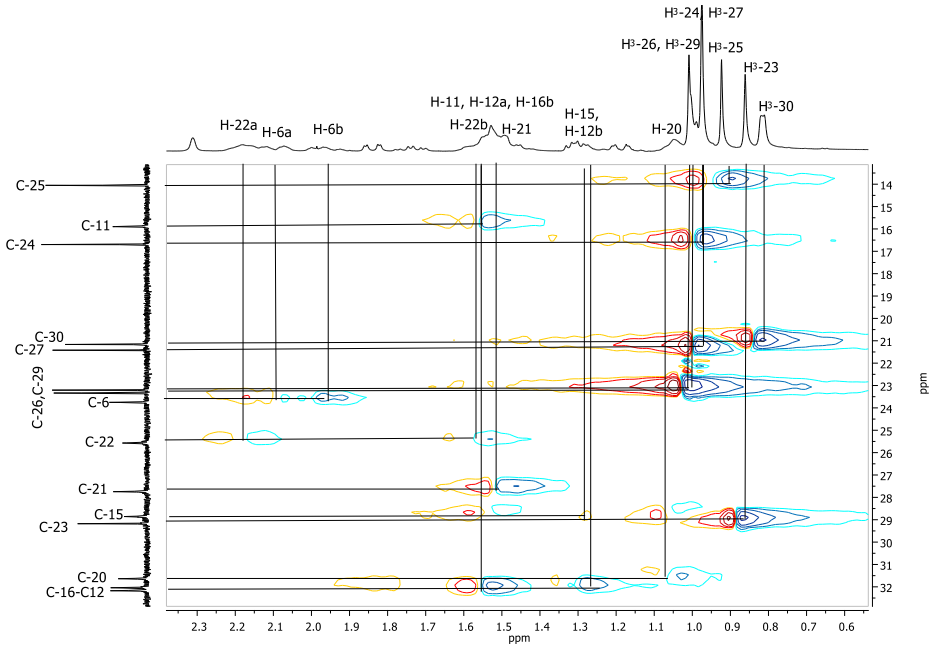

Figure S15c: Extended HSQC spectrum of callicarpifolic acid (**2**) in DMSO-d_6.

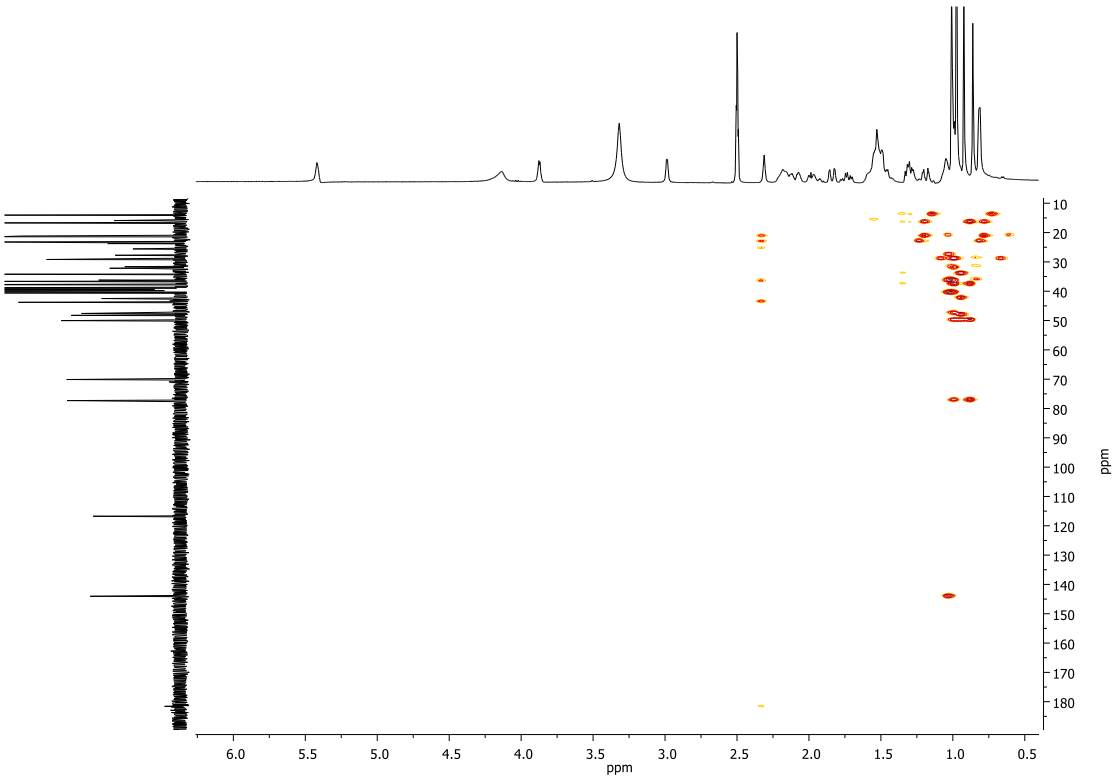

Figure S16: HMBC spectrum of callicarpifolic acid **(2)** in DMSO-d_6.

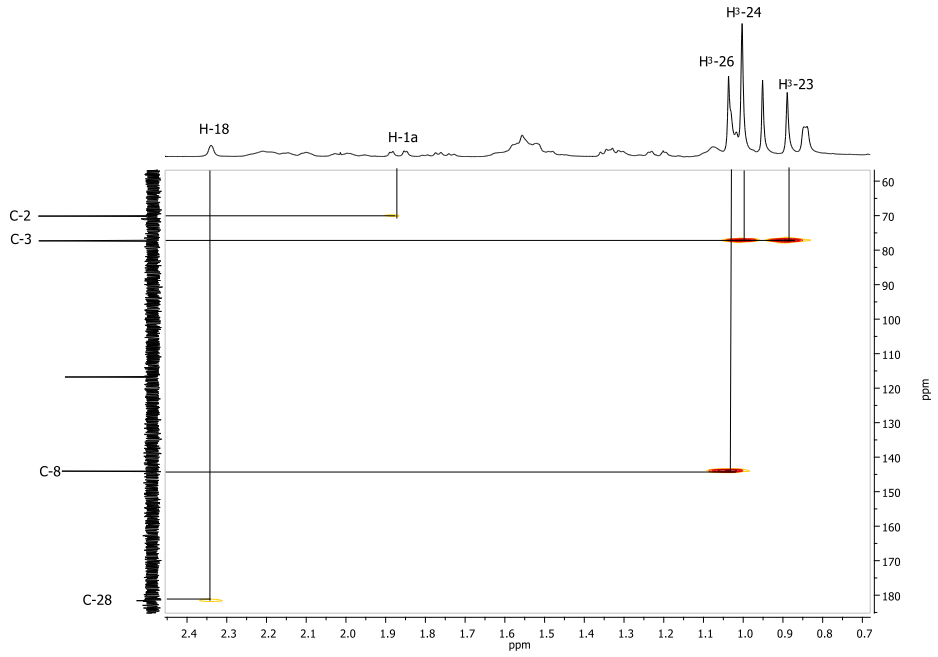

Figure S16a: Extended HMBC spectrum of callicarpifolic acid **(2)** in DMSO-d_6.

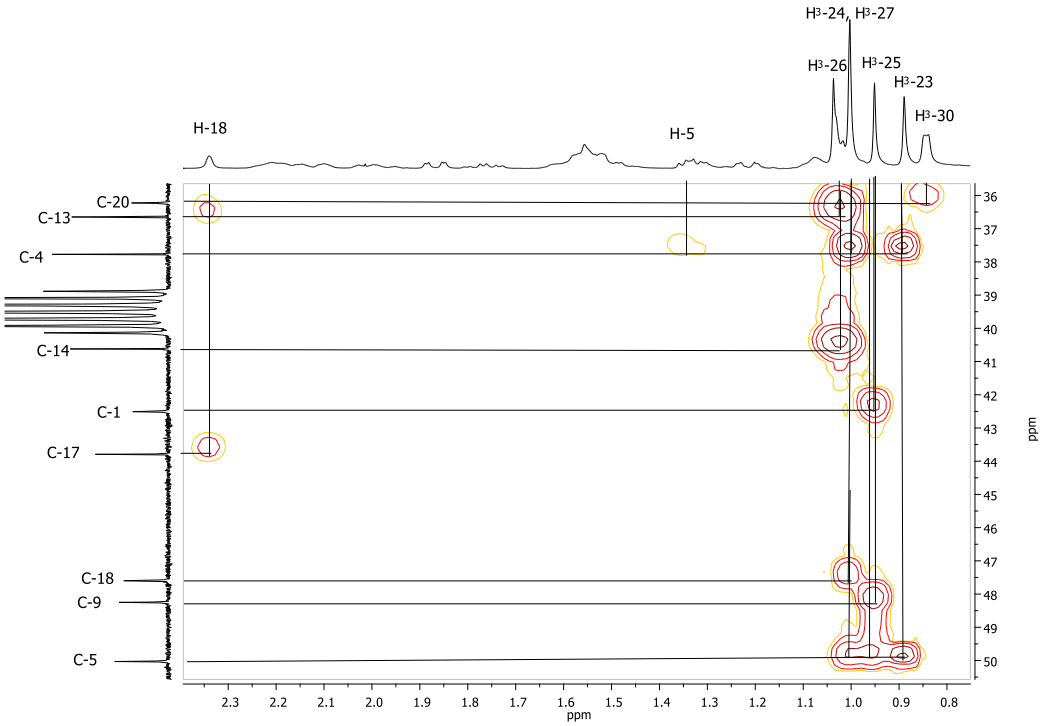

Figure S16b: Extended HMBC spectrum of callicarpifolic acid **(2)** in DMSO-d_6.

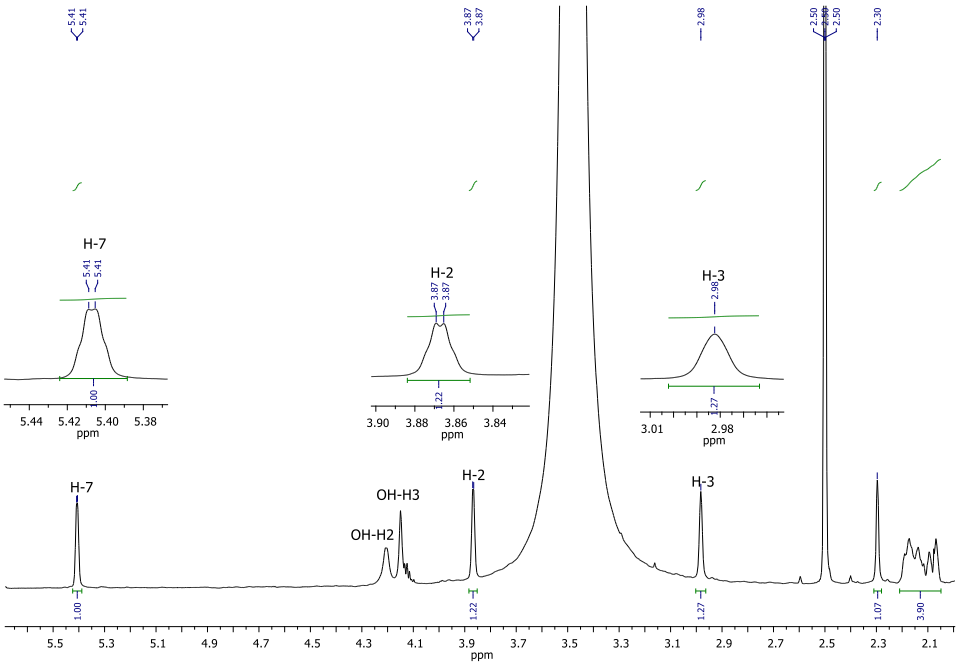

Figure S17: ^{1}H NMR spectrum of callicarpifolic acid **(2)** in DMSO-d_6 (700 MHz).

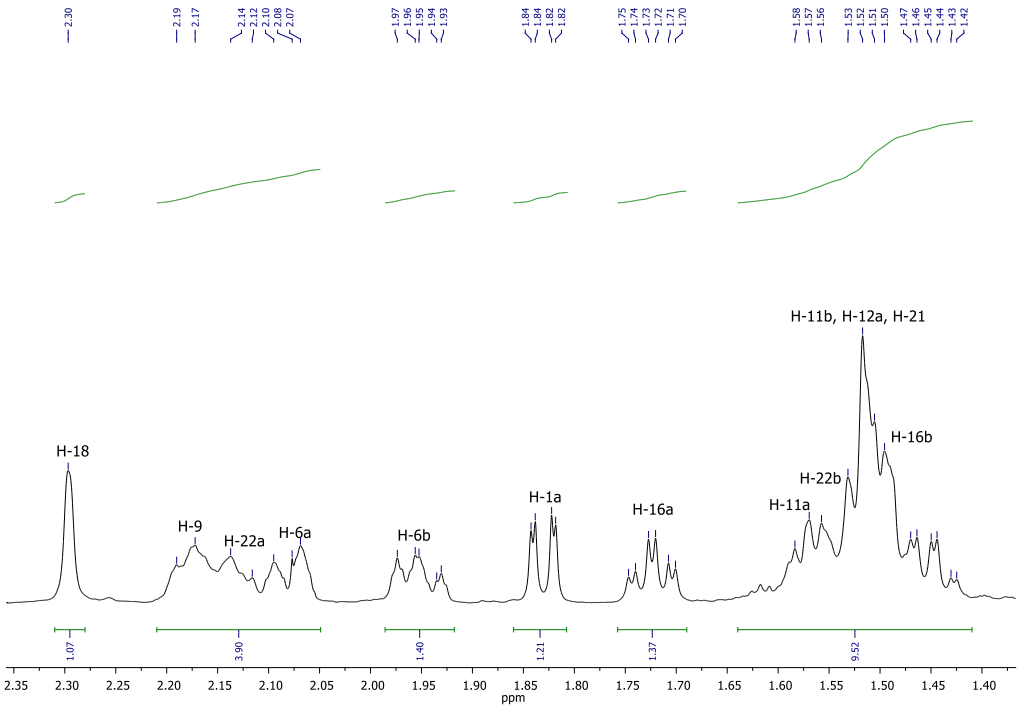

Figure S17a: ^{1}H NMR spectrum of callicarpifolic acid **(2)** in DMSO-d_6 (700 MHz).

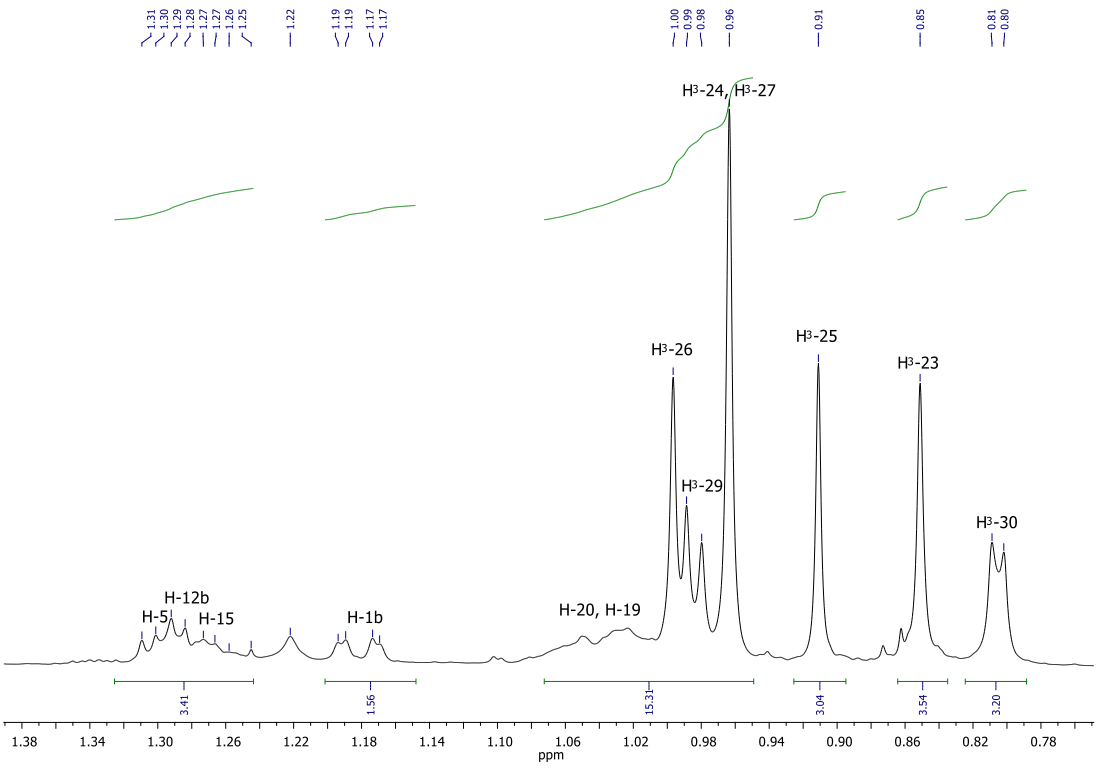

Figure S17b: ^{1}H NMR spectrum of callicarpifolic acid **(2)** in DMSO-d_6 (700 MHz).

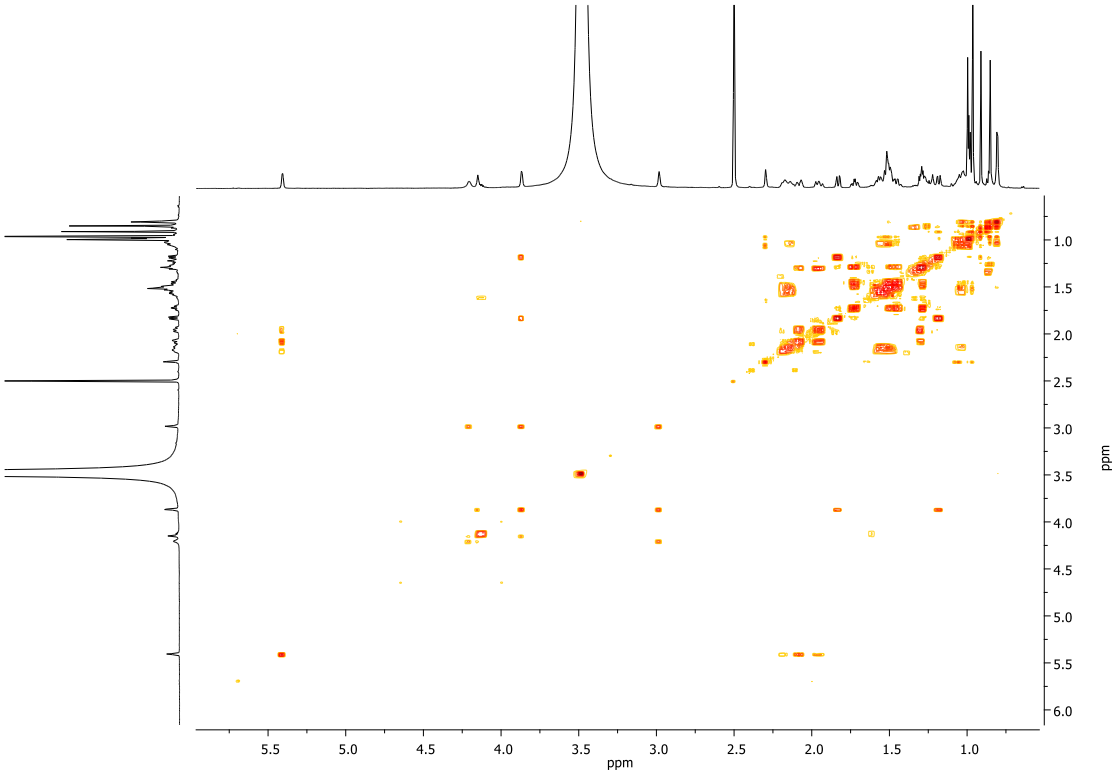

Figure S18: COSY spectrum of callicarpifolic acid (**2**) in DMSO-d_6.

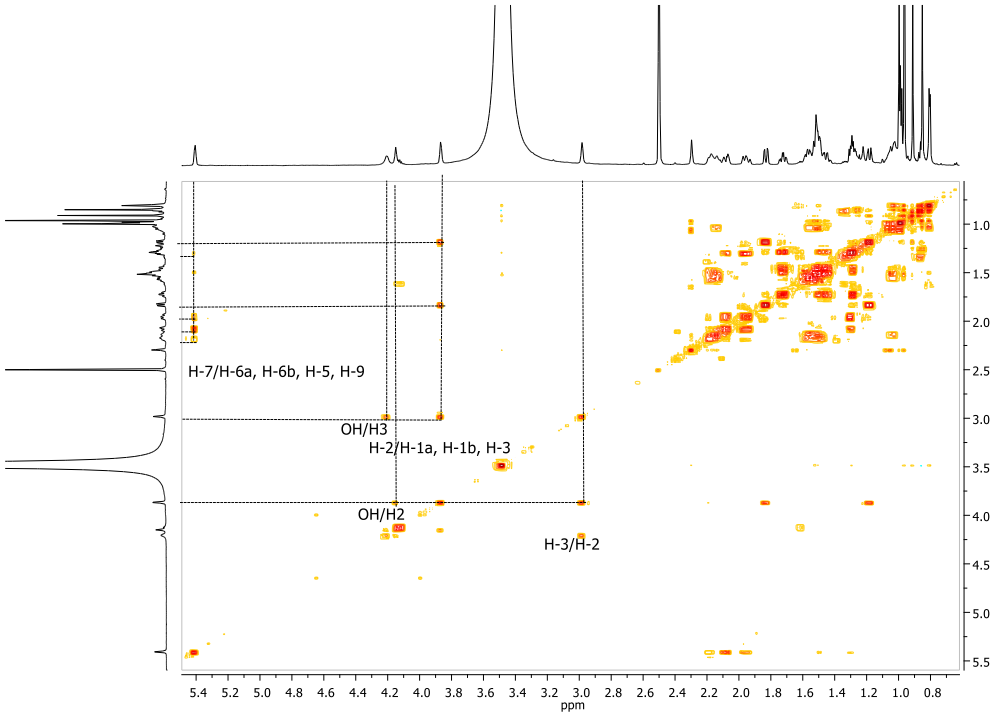

Figure S18a: Extended COSY spectrum of callicarpifolic acid (**2**) in DMSO-d_6.

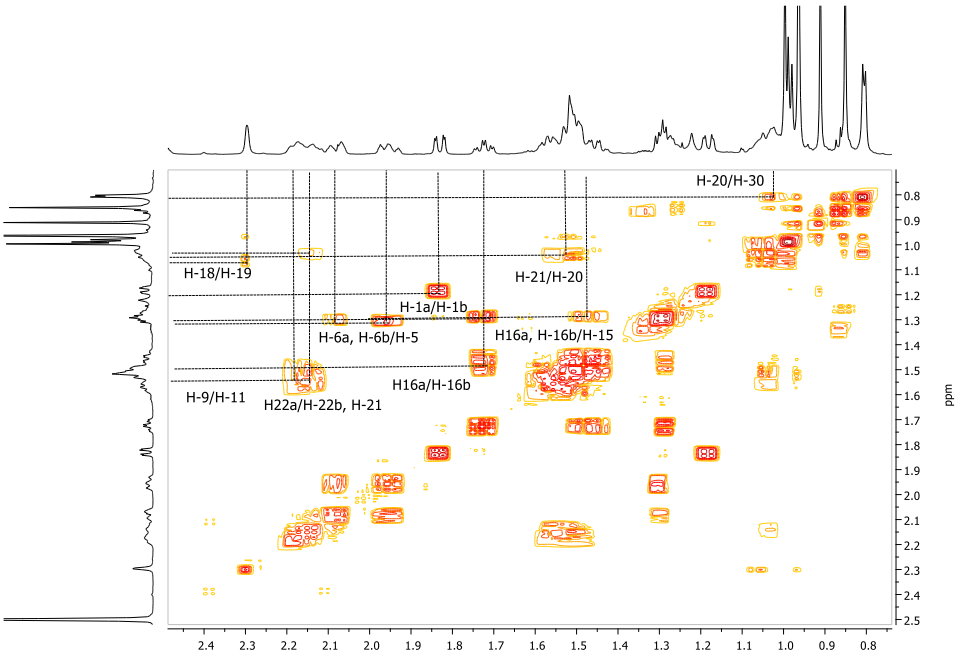

Figure S18b: Extended COSY spectrum of callicarpifolic acid (**2**) in DMSO-d_6.

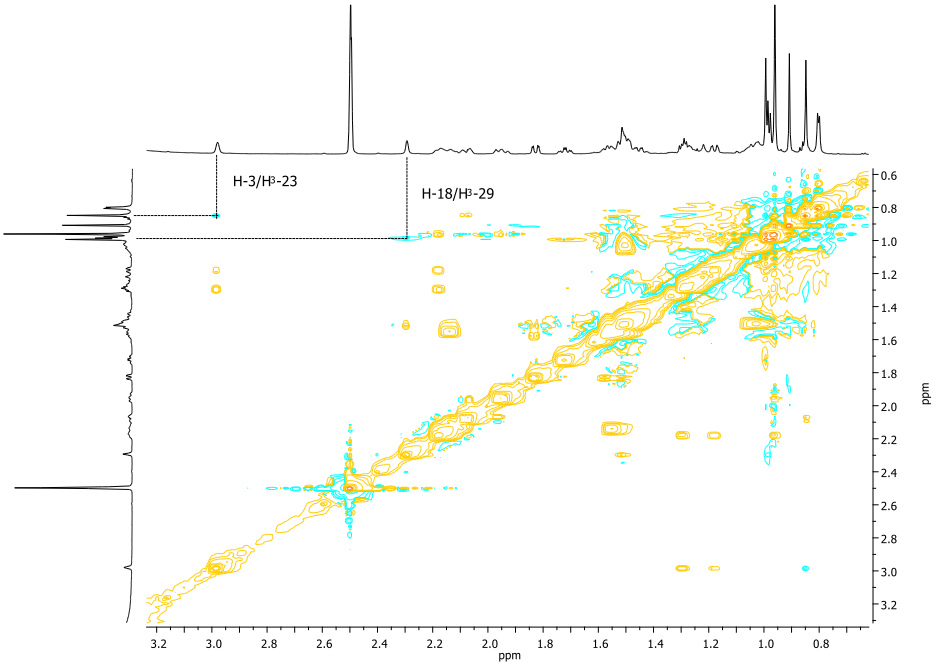

Figure S19: NOESY spectrum of callicarpifolic acid (**2**) in DMSO-d_6.

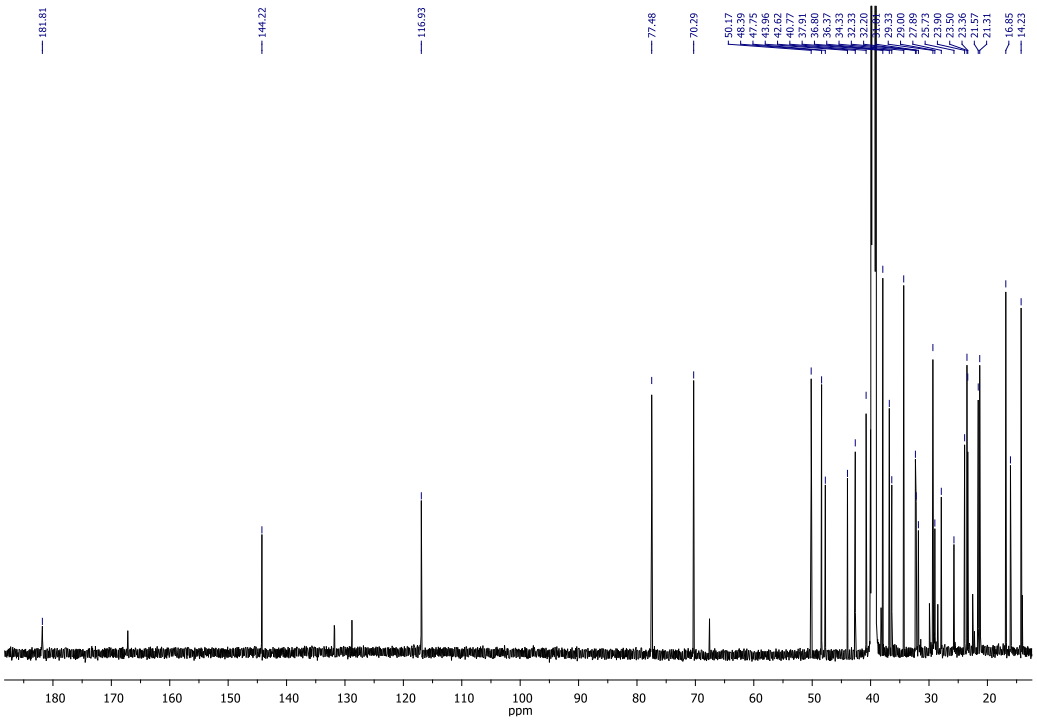

Figure S20: ^{13}C NMR spectrum of callicarpifolic acid (**2**) in DMSO-d_6 (175 MHz).

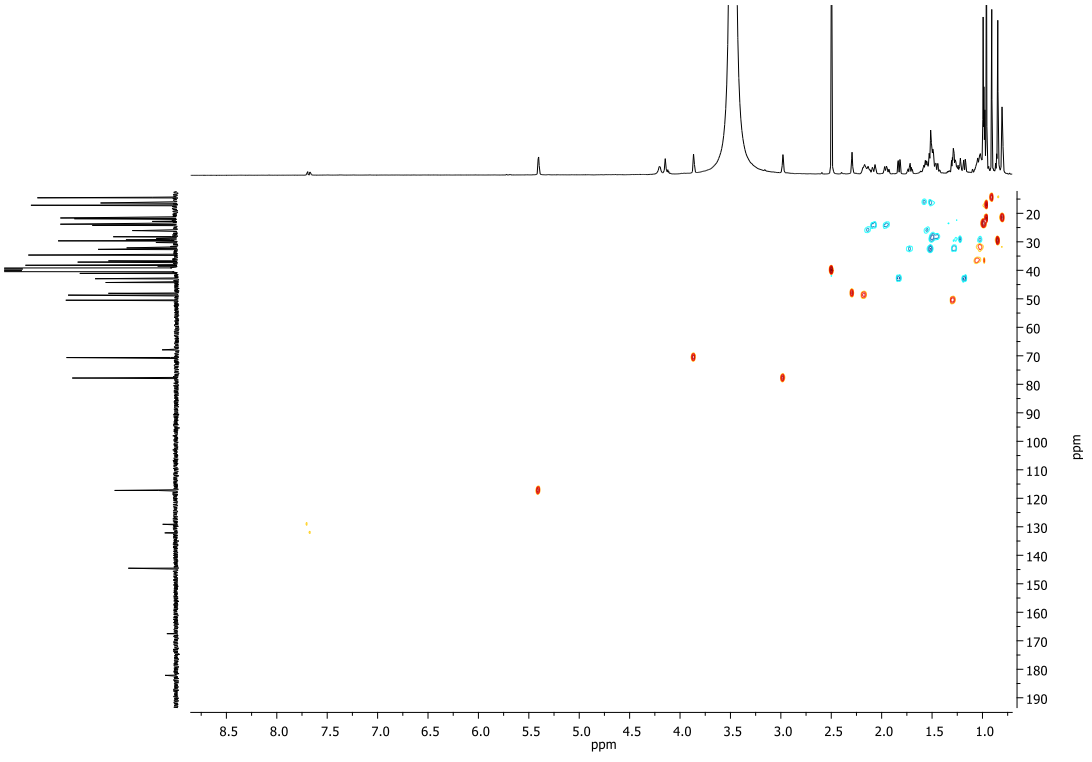

Figure S21: HSQC spectrum of callicarpifolic acid (**2**) in DMSO-d_6.

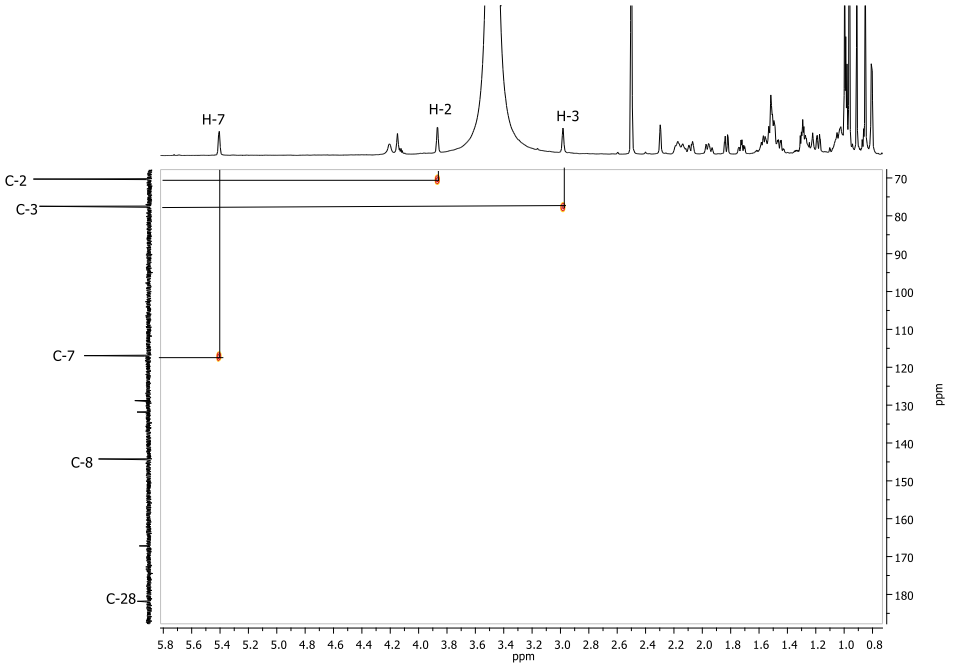

Figure S21a: Extended HSQC spectrum of callicarpifolic acid (**2**) in DMSO-d_6.

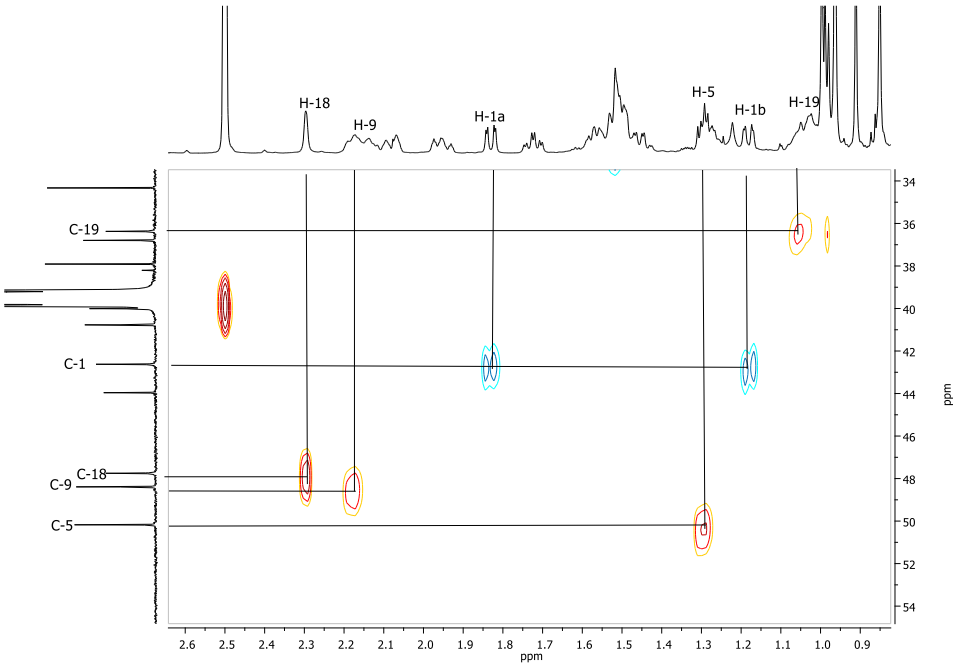

Figure S21b: Extended HSQC spectrum of callicarpifolic acid (**2**) in DMSO-d_6.

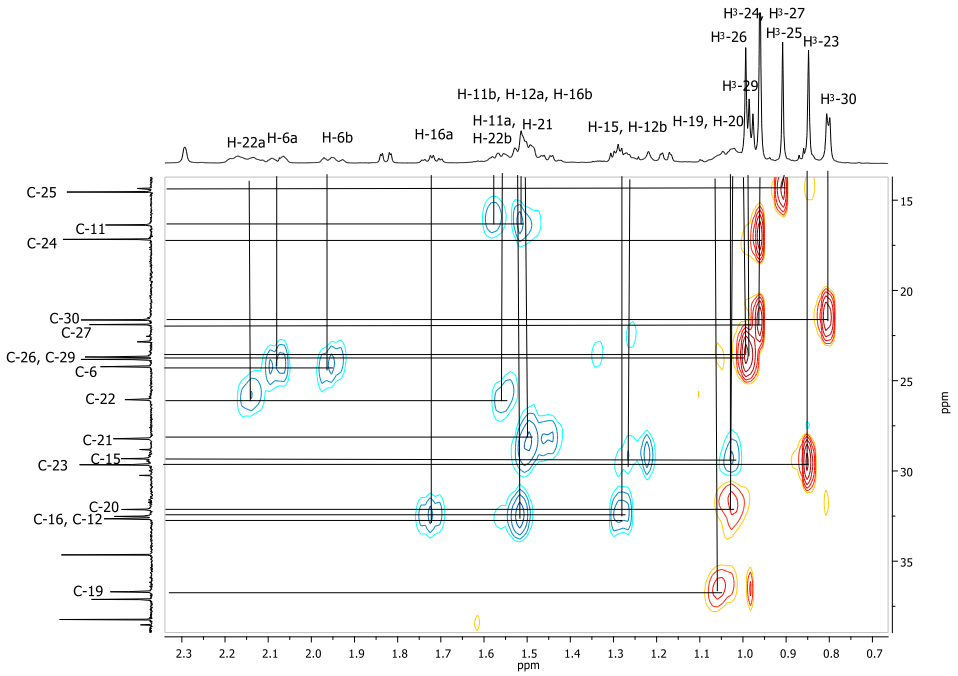

Figure S21c: Extended HSQC spectrum of callicarpifolic acid (**2**) in DMSO-d_6.

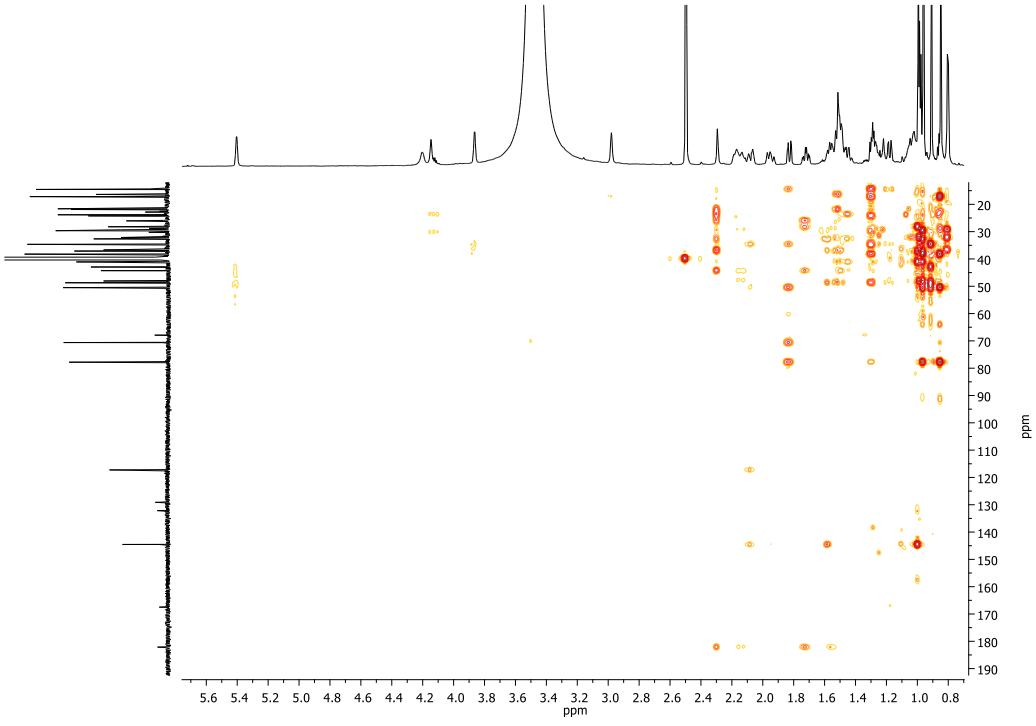

Figure S22: HMBC spectrum of callicarpifolic acid (**2**) in DMSO-d_6.

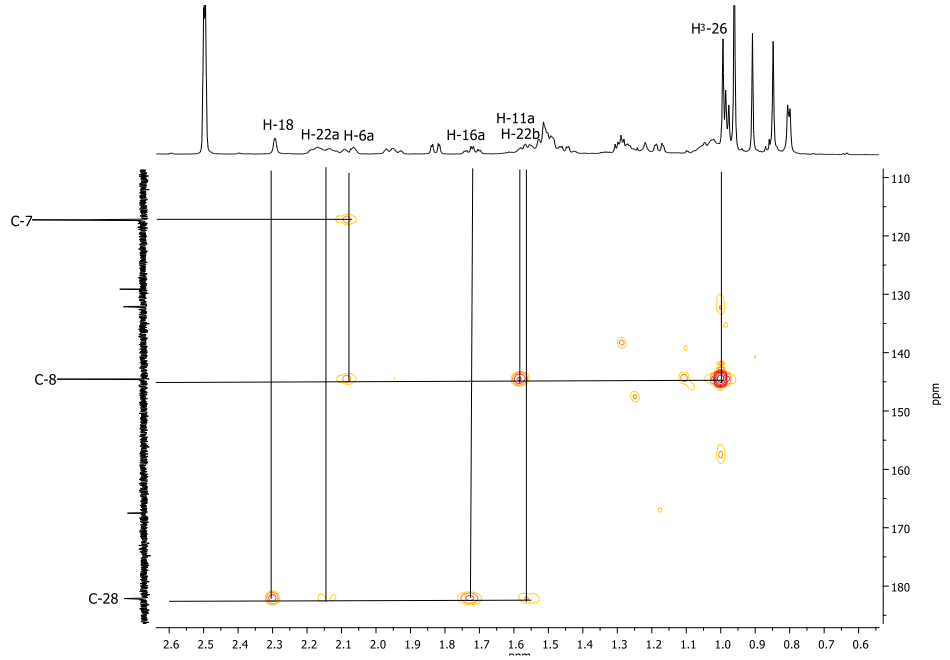

Figure S22a: Extended HMBC spectrum of callicarpifolic acid (**2**) in DMSO-d_6.

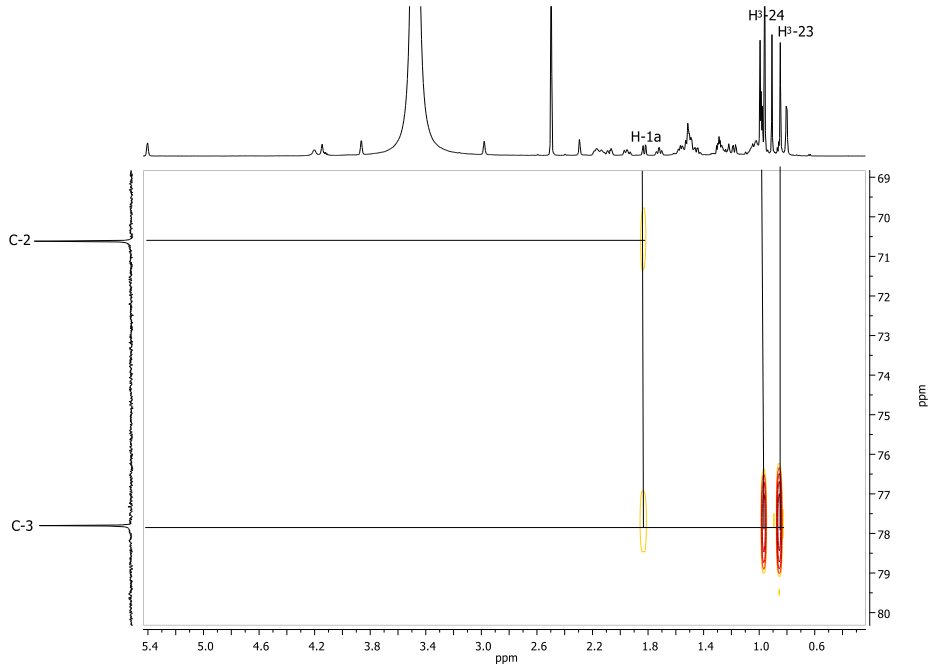

Figure S22b: Extended HMBC spectrum of callicarpifolic acid (**2**) in DMSO-d_6.

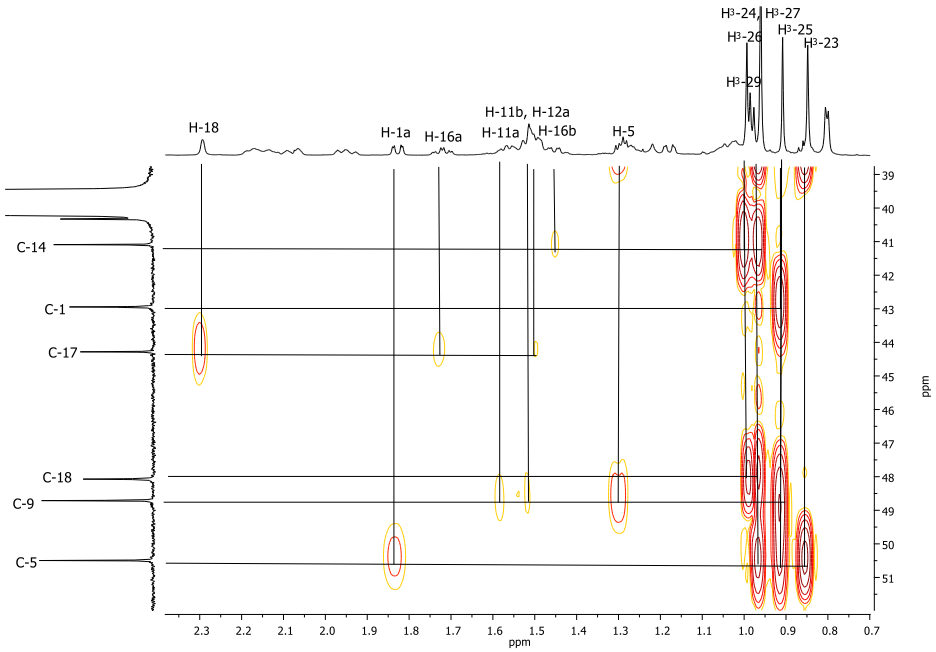

Figure S22c: Extended HMBC spectrum of callicarpifolic acid (**2**) in DMSO-d_6.

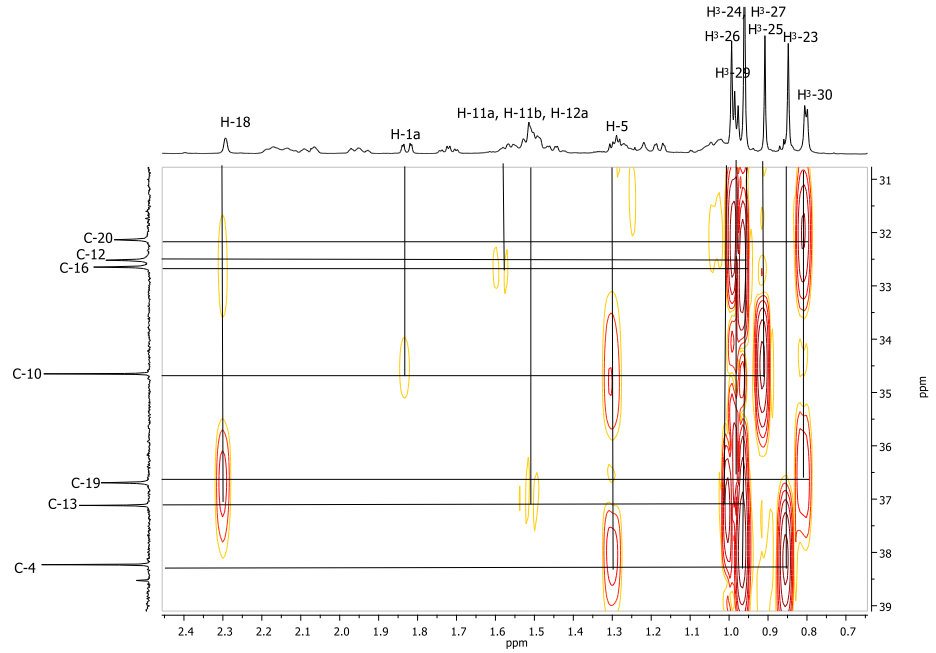

Figure S22d: Extended HMBC spectrum of callicarpifolic acid (**2**) in DMSO-d_6.

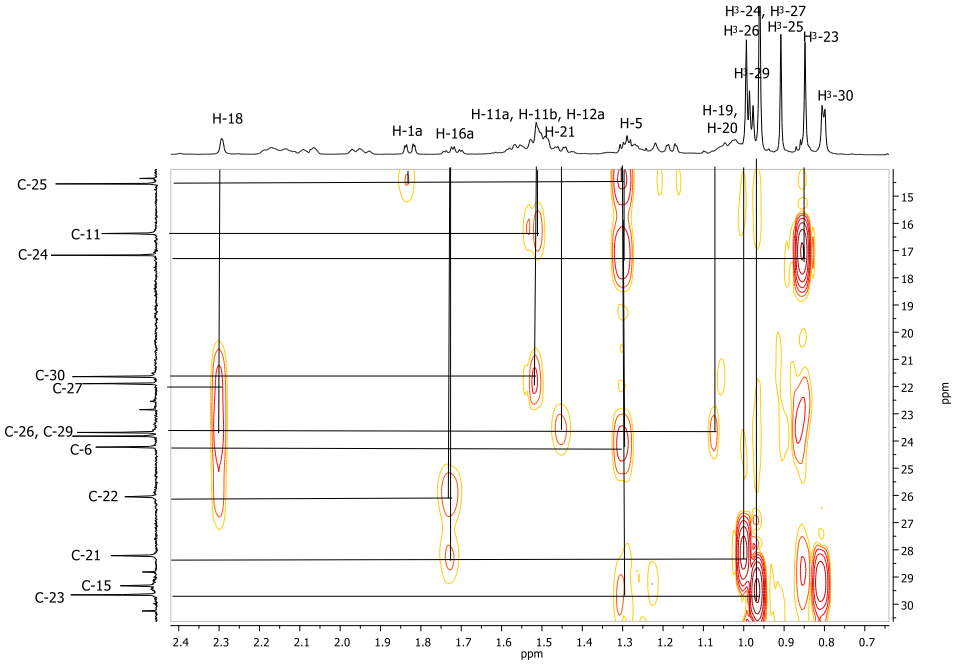

Figure S22e: Extended HMBC spectrum of callicarpifolic acid (**2**) in DMSO-d_6.

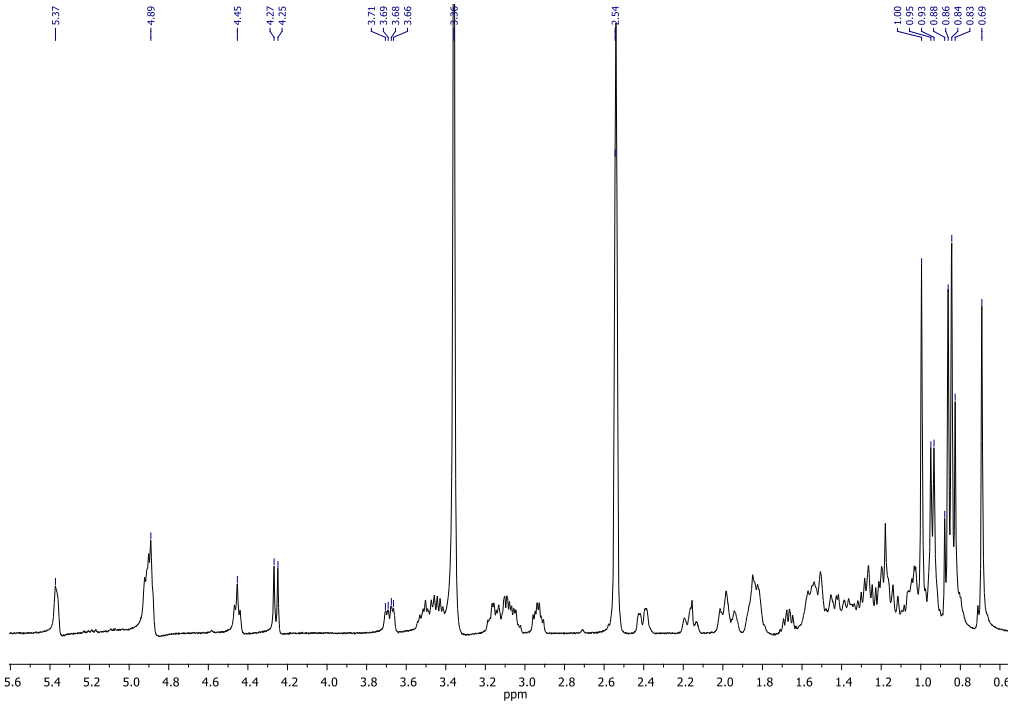

Figure S23: ^{1}H NMR spectrum of β-sitosterol glucoside (**3**) in DMSO-d_6 (300 MHz).

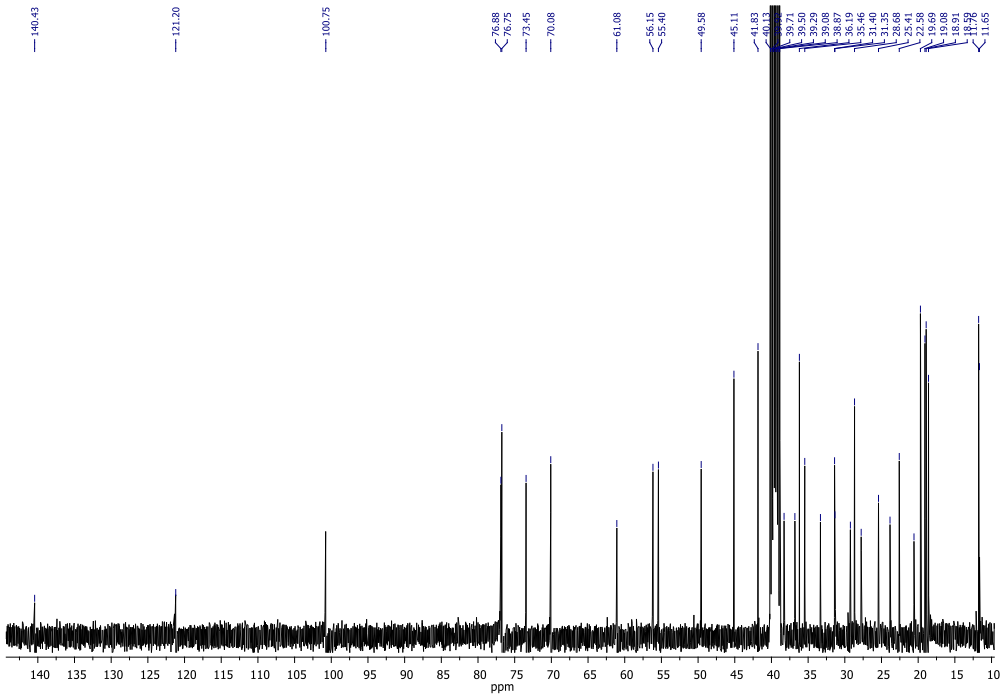

Figure S24: ^{13}C NMR spectrum of *β*-sitosterol glucoside (**3**) in DMSO-d_6 (75.4 MHz).

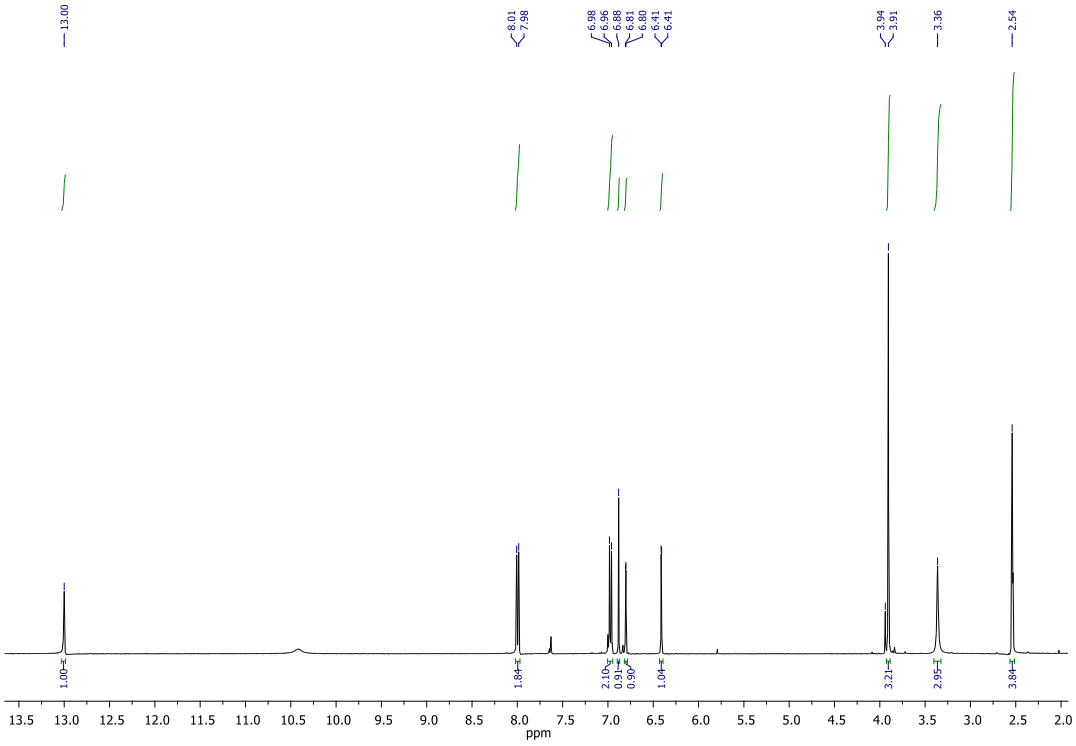

Figure S25: ^{1}H NMR spectrum of genkwanin (**4**) in DMSO-d_6 (300 MHz).

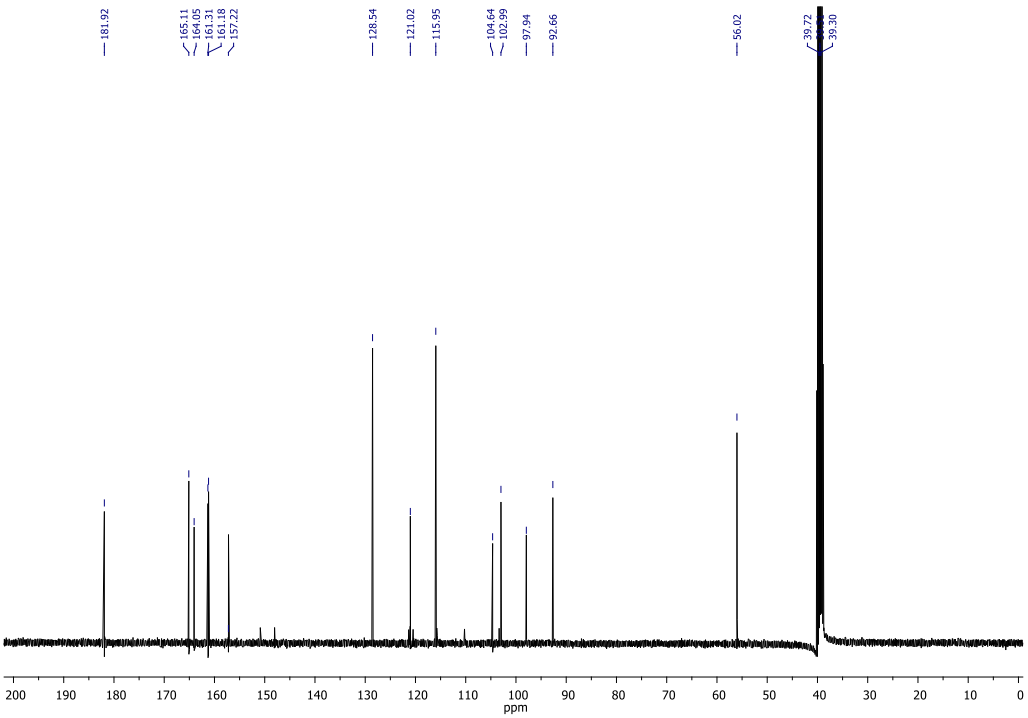

Figure S26: ^{13}C NMR spectrum of genkwanin (**4**) in DMSO-d_6 (75.4 MHz).

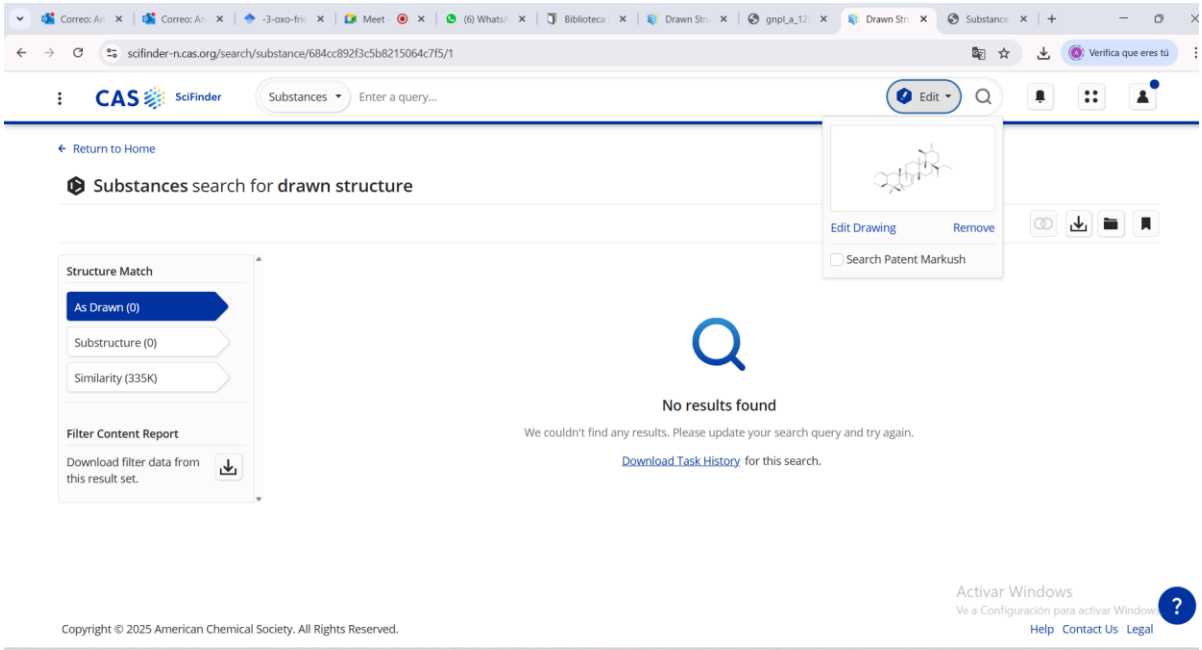

Figure S27: SciFinder research of callicarpifolic acid (**2**).

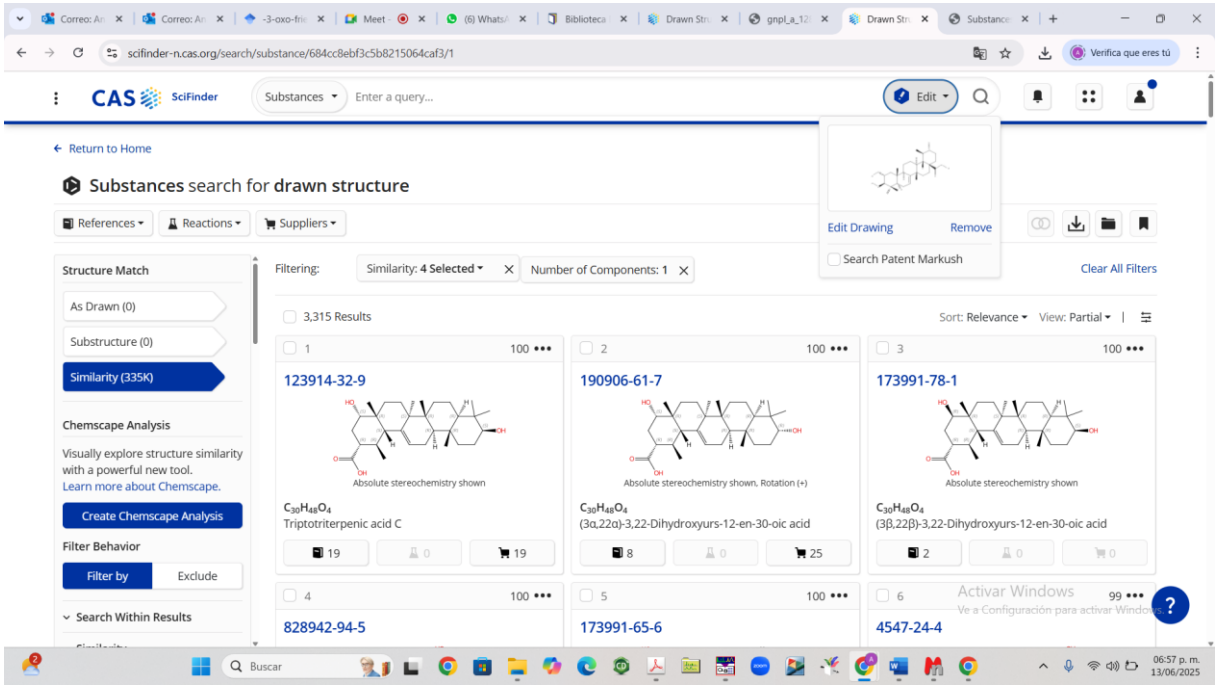

Figure S27a: SciFinder research of callicarpifolic acid (**2**).